INFORMATION TO USERS

While the most advanced technology has been used to photograph and reproduce this manuscript, the quality of the reproduction is heavily dependent upon the quality of the material submitted. For example:

- Manuscript pages may have indistinct print. In such cases, the best available copy has been filmed.
- Manuscripts may not always be complete. In such cases, a note will indicate that it is not possible to obtain missing pages.
- Copyrighted material may have been removed from the manuscript. In such cases, a note will indicate the deletion.

Oversize materials (e.g., maps, drawings, and charts) are photographed by sectioning the original, beginning at the upper left-hand corner and continuing from left to right in equal sections with small overlaps. Each oversize page is also filmed as one exposure and is available, for an additional charge, as a standard 35mm slide or as a 17"x 23" black and white photographic print.

Most photographs reproduce acceptably on positive microfilm or microfiche but lack the clarity on xerographic copies made from the microfilm. For an additional charge, 35mm slides of 6"x 9" black and white photographic prints are available for any photographs or illustrations that cannot be reproduced satisfactorily by xerography.

Khellaf, Abdallah

LATTICE DEFECT STUDIES OF HIGH QUALITY SINGLE CRYSTAL PLATINUM AND PALLADIUM

The University of Arizona PH.D. 1987

PLEASE NOTE:

In all cases this material has been filmed in the best possible way from the available copy. Problems encountered with this document have been identified here with a check mark __✓__.

1. Glossy photographs or pages _____
2. Colored illustrations, paper or print _____
3. Photographs with dark background _____
4. Illustrations are poor copy _____
5. Pages with black marks, not original copy _____
6. Print shows through as there is text on both sides of page _____
7. Indistinct, broken or small print on several pages ✓
8. Print exceeds margin requirements _____
9. Tightly bound copy with print lost in spine _____
10. Computer printout pages with indistinct print _____
11. Page(s) _____ lacking when material received, and not available from school or author.
12. Page(s) _____ seem to be missing in numbering only as text follows.
13. Two pages numbered _____. Text follows.
14. Curling and wrinkled pages _____
15. Dissertation contains pages with print at a slant, filmed as received ✓
16. Other _____

_____

_____

LATTICE DEFECT STUDIES OF HIGH QUALITY SINGLE CRYSTAL PLATINUM AND PALLADIUM

by

Abdallah Khellaf

A Dissertation Submitted to the Faculty of the

DEPARTMENT OF PHYSICS

In Partial Fulfillment of the Requirements
for the degree of

DOCTOR OF PHILOSOPHY

In the Graduate College

THE UNIVERSITY OF ARIZONA

1 9 8 7

THE UNIVERSITY OF ARIZONA
GRADUATE COLLEGE

As members of the Final Examination Committee, we certify that we have read the dissertation prepared by Abdallah Khellaf

entitled Lattice Defect Studies of High Quality Single Crystals Platinum and Palladium

and recommend that it be accepted as fulfilling the dissertation requirement for the Degree of Doctor of Philosophy.

Donald R. Huffman	April 20, 1987 Date
Ke Ching Hsu	20 April 1987 Date
Joseph J. Vuillemin	20 April 1987 Date
Hosny Mahmoud	April 20, 1987 Date
Roy W. Emerick	20 April 1987 Date

Final approval and acceptance of this dissertation is contingent upon the candidate's submission of the final copy of the dissertation to the Graduate College.

I hereby certify that I have read this dissertation prepared under my direction and recommend that it be accepted as fulfilling the dissertation requirement.

Roy W. Emerick
Dissertation Director

23 April 1987
Date

STATEMENT BY AUTHOR

This dissertation has been submitted in partial fulfillment of requirements for an advanced degree at The University of Arizona and is deposited in the University Library to be made available to borrowers under rules of the Library.

Brief quotations from this dissertation are allowable without special permission, provided that accurate acknowledgment of source is made. Requests for permission for extended quotation from or reproduction of this manuscript in whole or in part may be granted by the head of the major department or the Dean of the Graduate College when in his or her judgment the proposed use of the material is in the interests of scholarship. In all other instances, however, permission must be obtained from the author.

SIGNED: A. Khellaf

DEDICATION

In memory of my father.

To my mother.

To my brother Nadji.

ACKNOWLEDGEMENTS

I would like to express my gratitude to my thesis advisor, Professor Roy M. Emrick, for his encouragement and advice throughout the course of this work. Secondly, I would like to thank Professor Joseph J. Vuillemin for many helpful discussions. Also, I would like to thank Professor Royal W. Stark for the helpful discussions on the high temperature measurements and for the use of his equipments.

I would like to take this opportunity to thank Mr Frank Wadleigh and Mr Rodney Lowell for their encouragements throughout the years. Much appreciation goes to Ali and Ahmed Boufelfel who went out of their ways to help in any way they could. Harry Schmitt, Chu Xing Chen, John Kupfer, Tom Whittemore and Les Vanyo have provided encouragement, friendship and amusing diversions.

Finally, the faculty and the staff of the physics department have been supportive and made me feel at home. For this I am very grateful.

TABLE OF CONTENTS

TABLE OF CONTENTS---Continued

LIST OF ILLUSTRATIONS

LIST OF ILLUSTRATIONS--Continued

LIST OF TABLES

ABSTRACT

An improved quenching technique is described. This technique allows samples to be quenched at slow quenching rates without introducing unwanted dislocations during quench. High quality platinum single crystals 1 mm in diameter have been quenched from temperatures between 900°C and 1550°C using this technique. The data have been analysed and discussed using a sink model for vacancy loss proposed by Emrick. The formation energy was found to be (1.30 $\pm$ 0.03) eV. The entropy of formation and the concentration of vacancies at the melting point have been determined to be respectively (0.42 $\pm$ 0.11)k and (9.4 $\pm$ 0.7)10^{-4}.

High purity palladium single crystals have also been quenched using the same technique.

Due to the need for a temperature scale, measurements of the electrical resistance of an ultra pure palladium single crystal have been made to a temperature within 100°C of the melting point. These, along with measurements of the liquid palladium resistivity, are reported. The results are discussed and compared to previously reported values.

CHAPTER I

INTRODUCTION

1. Generality

Many of the important properties of crystals are strongly dependent upon the nature and concentration of various defects which are present in the crystals. A knowledge of the equilibrium concentration of defects and their temperature dependence is necessary for the understanding and control of the crystal properties related to these defects.

Defects, which are perturbations of the ideal crystal structure, include point defects, dislocations or linear defects and grain boundaries or surfaces. Defects that extend over only a few atomic distances are called point defects. Figure 1.1 shows some of these defects. In metals, there are two kinds of point defects:

1. Intrinsic point defects such as vacancies, interstitials and their clusterings. Vacancies are empty lattice sites. An interstitial is an atom in a position which is not a normal lattice site.
2. Extrinsic point defects involve foreign atoms that may be placed either at a regular lattice site or in between the normal sites (at an interstitial site).

Dislocations are the most common of the line defects in

Figure 1.1 Two dimensional square lattice illustrating the most common types of point defects.

(V) vacancy, (D) divacancy, (T) trivacancy and (I) interstitial in a crystal.

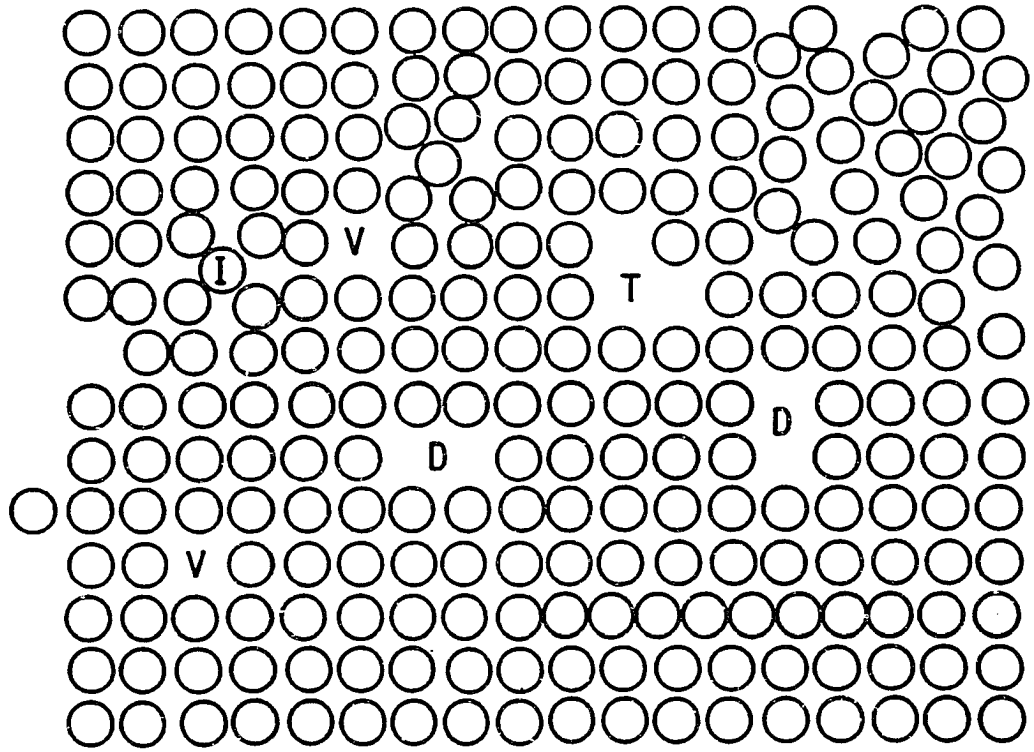

Figure 1.1 Two dimensional square lattice illustrating the most common types of point defects.

metals. They mark the boundary between portions of the lattice which are slipped one lattice spacing relative to the adjacent region. Edge dislocations and screw dislocations are examples of line dislocations. An edge dislocation arises when a half plane of atoms is inserted in a regular array of atoms as shown in Figure 1.2. A screw dislocation occurs when one part of a crystal has been partially sheared from another part. The dislocation density is defined as the total length of dislocation line per unit volume of crystal. It varies from 10^3 cm/cm^3 in carefully grown crystals to 10^{12} cm/cm^3 in heavily deformed crystals.

This discussion will be limited to vacancies and their interactions with dislocations in metals. Dislocations play an important role in maintaining the equilibrium concentration of point defects (Seidman and Balluffi 1966). They serve as the primary bulk sources and sinks for vacancies both thermally and mechanically. Surfaces also play a role, for, vacancies may be created by diffusion of an atom from its lattice site into an unoccupied site on the surface or into a grain boundary.

Vacancies are created in the bulk by edge dislocation climb. In this process, the vacancies are generated (or annihilated) at jogs.

Jogs are steps in the edge of the extra plane of atoms. Figure 1.3 shows a jog. It can be noticed that the atom at the jog is the least tightly bound to the extra plane and an atom arriving at a jog can form two bonds with nearest neighbors.

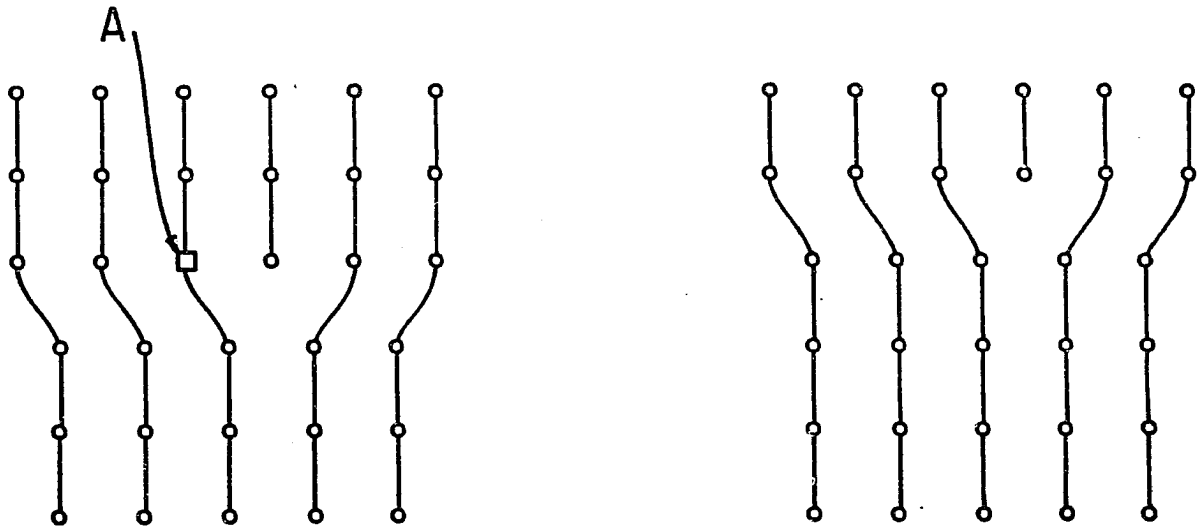

Figure 1.2 An edge dislocation as a sink for vacancies.

The edge dislocation is created by the insertion of the extra plane of atoms from the top. The dislocation line is perpendicular to the page along the edge of the extra plane. Imagine that the dislocation line jumps one lattice constants to the right on the lattice plane above the page. That is, there is a jog in the dislocation line (see fig 1.3). As the vacancy A is absorbed (atom from extra plane moves into the vacancy) the jog moves one atomic spacing into the page.

Figure 1.3 An edge dislocation as a source of vacancies.

Motion of an atom from plane C to the jog on plane B results in the displacement of the jog one atomic distance to the right. A vacancy is created at * on plane C.

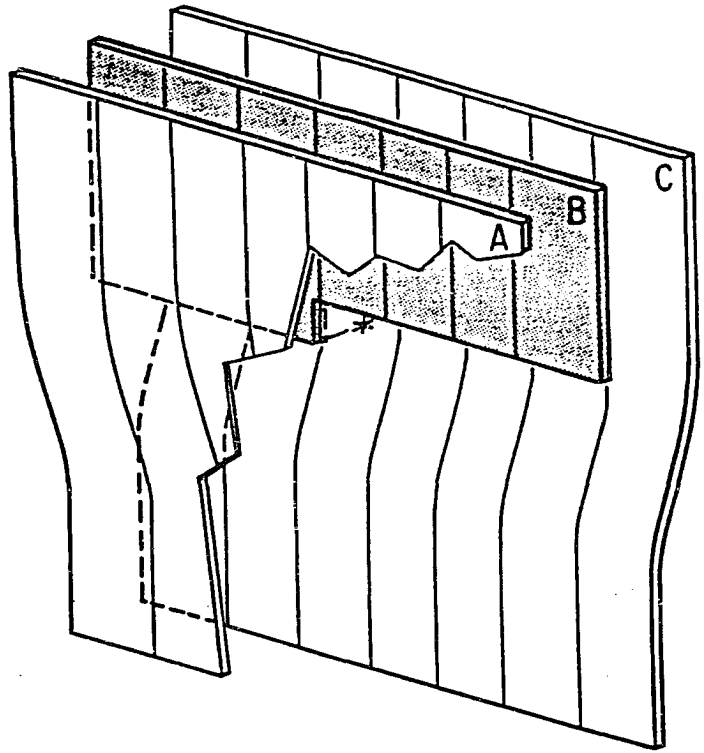

Figure 1.3 An edge dislocation as a source of vacancies.

Thus jogs are favorable spots for emission and absorption of vacancies. A vacancy on a plane A is annihilated when the atom at the jog on plane B jumps into the vacant lattice site. This results in the jog moving one atomic spacing along the dislocation to the left. Conversely a vacancy is created on plane C for example when an atom from this plane jumps to the jog. This results in the jog moving one atomic spacing along the dislocation line to the right. This process is reversible and the direction of motion of a jog depends on the vacancy concentration gradient in the crystal. If there is no gradient, vacancies are created and annihilated with equal frequency. However if we have for example an excess of vacancies, the rate of their arrival at jogs increases, therefore increasing their annihilation.

In metals, mechanical deformations occur by motion of dislocations. In this case, a non-equilibrium concentration of vacancies is irreversibly produced by edge dislocation climb. In this process, as the dislocation jumps from one glide plane to the next, the vacancies are created or absorbed at jogs.

2 Equilibrium Vacancy Concentrations

Vacancies may be regarded as a dilute solution of vacant lattice sites in the host crystal. In order to create a vacancy, an atom has to be brought from its regular site to a surface site. But since there are many different indistinguishable sites from which the atom may be removed, there is an entropy of mixing that lowers the total free energy of the system even though the

internal energy associated with the creation of vacancies increases. The entropy of mixing due to n vacancies can be calculated by considering the number of ways Ω in which n vacancies can be arranged on N lattice sites. Such number of ways is given by the binomial coefficient:

$$\Omega = \frac{N!}{(N-n)!n!}$$

so that the entropy of mixing is given by:

$$S_{mix} = k \ln \Omega \quad .$$

By using Stirling 's theorem we obtain:

$$S_{mix} = k\{N\ln(n) - (N-n)\ln(N-n) - n\ln(n)\} \qquad (1)$$

The free energy of formation of a vacancy is :

$$F_f = E_f - TS_f \qquad (2)$$

where E_f is the energy of formation of a single vacancy which is equal to the work done to bring an atom from a regular lattice site to a sink, and S_f is the entropy of formation which results from the change in lattice vibration frequencies when a vacancy is created.

The total free energy is (Flynn 1972):

$$\Delta F = nF_f - TS_mix \qquad (3)$$

From equations (1) through (3) we get

$$\Delta F = nE_f - nTS_f - kT[N\ln N - (N-n)\ln(N-n) - n\ln n] \qquad (4)$$

The condition for thermal equilibrium is that the free energy is minimum, i.e.,

$$\frac{\partial(\Delta F)}{\partial n}\Big|_{n=n_0} = 0$$

So that

$$\frac{n_0}{N-n_0} = \exp(S_f/k)\exp(-E_f/kT)$$

even at the melting point $n_0 \ll N$ so that the concentration of vacancies is given by:

$$C_v = \frac{n_0}{N} \simeq \exp(S_f/k)\exp(-E_f/kT)$$

For a number of fcc metals, the energy of formation E_f has been found to be of the order of 1 eV, and the equilibrium concentration of vacancies C_v near the melting point is usually between 10^{-4} and 10^{-3}. Typical values for these parameters for some of the fcc metals are shown in Table 1.1.

The observation and study of the equilibrium concentration of vacancies can be carried out in two distinct ways:

1. By direct observation.
2. By monitoring the change in some physical properties sensitive to the presence of the point defects.

Direct observation of point defects is useful because of the capacity of the direct resolution of the defect structure. Direct observation is accomplished by using microscopic techniques such as field ion microscopy. Unfortunately, because of the atomic size of the point defects, direct observation is

Table 1.1: Typical formation energies and concentrations of vacancies at the melting point in fcc metals.

Metal	E_f(eV)	$C_v(T_m)$ (10^{-4})	Method	Reference
Au	0.97	7.2	D	Simmons and Balluffi (1963)
Ag	0.9	1.7	D	Simmons and Balluffi (1960)
Al	0.76	9.4	D	Simmons and Balluffi (1963)
Cu	1.17	2.0	D	Simmons and Balluffi (1960)
Ni	1.22±.07	4 - 6	PA	Dlubek et al (1977)
Pt	1.32	10.2	PA	Schaeffer (1982)
	1.45	26.	D	Kopan (1965)

D : Dilatometry
PA: Positron annihilation

difficult to achieve.

Many physical properties are affected in various ways by the presence of point defects. For example point defects and their strain fields around them scatter electrons and thus introduce an increase in the electrical resistivity. They also introduce a change in density and lattice parameters. Because of their energy of formation they increase the specific heat of the sample. Mechanical property changes, such as hardness, are caused in the sample by the interaction of point defects and dislocations. All these changes can be used to investigate the nature, concentration, mobility and interactions of the point defects.

The experimental techniques which have successfully been used to study the equilibrium concentration of point defects and its temperature dependence, represented by the energy of formation, include both thermal equilibrium and non-equilibrium methods.

The thermal equilibrium experiments include differential dilatometry, calorimetry and positron annihilation spectroscopy. These kinds of experiments are usually carried out at high temperature, with high demands on experimental equipment. The samples are also susceptible to contamination. The main difficulty to be overcome in thermal equilibrium experiments is the elimination of the large background signal due to the defect free crystal.

The non-equilibrium experiments attempt to trap the

equilibrium defect population by fast cooling (quenching) for observation at much lower temperatures. They include resistometry and field ion microscopy. The major problems associated with this method are the loss of vacancies and the perturbation of their distribution.

In the following sections, the most frequent experimental approaches to the determination of the concentration of vacancies and the energy of formation will be reviewed. Of interest here is the resistivity measurement after quenching. The validity of this technique as a tool to investigate vacancies will be discussed. Finally the specific goals of this thesis will be outlined.

3. Differential Dilatometry

The differential dilatometry experiment is the only one that can provide direct values of the concentration of vacancies in metals under thermal equilibrium condition. Simmons and Ballufi (1960,1962,1963) were the first to report precise measurements on aluminum, gold and silver using this technique.

This method is based on the comparison of the thermal relative change, $\Delta a/a$, of the lattice parameter with that of the bulk crystal, $\Delta L/L$, over a temperature range extending to the melting point. In the experiment the macroscopic dimension change, ΔL, is measured with an interferometric method and the lattice parameter change, Δa, with an x-ray diffraction method. These measurements are made simultaneously on the same sample, at

the same temperature.

If a vacancy is introduced in a crystal, the crystal volume increases by a fraction of an atomic volume. On the other hand, the introduction of an interstitial decreases the crystal volume by a fraction of an atomic volume. Relaxation of the crystal around a vacancy or an interstitial and thermal expansion affect the bulk crystal dimension and the lattice parameters equally. The effect of the introduction of a point defect is then responsible for the difference between the relative change of the lattice parameters and the relative change in the bulk dimension. Thus this difference is directly related to the concentration of point defects which can be expressed by:

$$C_{ef} = C_V - C_I = 3(\Delta L/L - \Delta a/a) \qquad (6)$$

where C_V is the concentration of vacancies and C_I is the concentration of interstitials. The above expression is valid for cubic crystals. For other crystals it is necessary to measure the sample and the lattice parameter expansions along more than one crystallographic direction.

If C_{ef} can be accurately measured over a sufficiently broad temperature range, this method can be used in conjunction with equation (5) to obtain the energy of formation E_f. From equation (5) we see that an Arrhenius plot of C_{ef} versus the inverse of the absolute temperature will yield a staight line with slope-E_f/k. Unfortunately this method has not yet been able to provide

accurate values for the energy of formation. The uncertainty in Ef varies from at least 5 % to above 10 %.

The major difficulty associated with this method is the extreme accuracy required in the measurements over a wide range of temperature. Since the measurement involves small differences between large quantities, extreme precision in $\Delta L/L$ and $\Delta a/a$ is required. Even though interferometry techniques allow for a high precision of sample dimension changes, the sensitivity of the x-ray techniques used for the measurements of lattice parameter is still limited. This means that the measurements are good only over a narrow range of temperature close to the melting point.

4 Positron Annihilation

Positrons are produced by the decay of radioactive sources such as ^{22}Na. After the positron emission, the nucleus emits a 1.28 MeV photon which serves as a birth signal for the positron. After being injected into the sample, the positron first thermalizes. Then, after living in thermal equilibrium for some mean lifetime, it annihilates with an electron into two gamma rays. At the end of the 1960's it was noticed that heating the sample to higher temperatures caused a change in the positron lifetime. Mackenzie et al (1967) were the first to link this effect to the thermally induced vacancies, and Brandt (1967) the first to propose a model to explain the results. The great sensitivity of positrons to vacancies in metals, even to a concentration of the

order of 10-6 , arises from the trapping of the positrons in vacancies. Because of this sensitivity, measurements can be carried out over a larger range of temperature than with differential dilatometry.

Three experimental techniques, positron lifetime, angular correlation and Doppler broadening, have been used to study vacancies in thermal equilibrium.

4.1. Positron Lifetime

The lifetime of the positron is the time delay between the birth and the annihilation gamma rays. The lifetime of positrons is characteristic of each material and varies from 100 to 500 psec.

The lifetime can be measured experimentally using fast timing techniques. The measurements yield information about the total electron density in the region of positron-electron annihilation. In a sample with vacancies, positrons see the vacancies as strong attractive centers. After entering the sample and being thermalized, the positron could either drift freely through the lattice or it could become trapped in a vacancy. Since the local electron density in a vacancy is much lower than in a perfect lattice, the positron lifetimes associated with annihilation of positrons localized in vacancies, τ_T , are much longer than those associated with annihilation in vacancy free lattice, τ_L . In the trapping model the mean lifetime , $\bar{\tau}$, is given by: $\bar{\tau} = \tau_L \frac{1+\tau_T \sigma C_v}{1+\tau_L \sigma C_v}$

where σ is the rate of positron trapping of a vacancy and C_V is the concentration of single vacancies.

τ_L can be obtained from measurements at low temperature, since at low temperature $\bar{\tau} = \tau_L$. τ_T can be measured at temperature close to the melting point, since most of the positrons are trapped . $\bar{\tau}$ can be measured at intermediate temperatures. The energy of formation of vacancies E_f of single vacancies can be obtained from the slope of the Arrhenius plot of $\frac{\bar{\tau}-\tau_L}{\tau_T-\bar{\tau}}$ as a function of 1/T.

Lifetime measurements are very demanding on equipment and are based on several assumptions, some of which require more examination. The long measuring time required can be a problem especially if the sample has a high vapor pressure.

4.2. Angular Correlation

Since the momentum of the center of mass of the annihilating positron-electron pair is not zero, the annihilation gamma rays will not be emitted at 180° . The angular deviation from 180°, $\delta\theta$, is proportional to the transverse component of the momentum. The line shape of the angular distribution, $\delta\theta$, reflects then the momentum distribution of the electrons.

Measurements of angular correlation accomplished by means of movable NaI detectors are characterized by the angular distribution which is usually defined by one of a number of shape parameters F of the experimental curve such as peak heights.

In vacancies the local fraction of high momentum electron states is reduced relative to lower momentum electron states, so the angular distribution will be narrower for positron annihilated in vacancies. Equations similar to the trapping model can be used to interpret data from angular correlation experiments.

Even though angular measurements are faster and easier to perform than lifetime measurements, they require relatively strong positron sources and more elaborate data deconvolutions.

4.3. Doppler Effect

Since the electron-positron pair has a momentum different from zero, its motion causes a Doppler shift in the energy of the annihilation gamma rays measured in the laboratory system. The energy shift , δE, from 511 keV of each gamma ray is proportional to the longitudinal component of the momentum. The line shape of the Doppler shift reflects then the momentum distribution of the electron.

Measurements of Doppler broadening with lithium drifted germanium detectors or with intrisic germanium detectors are characterized by the distribution of the energy shift δE. As in the angular distribution measurements, the distribution of the curve is characterized by a shape parameter F such as the full width at half maximum.

As in the case of angular correlation measurements in the study of defects, because of the dominance of the low momentum electron states in a vacancy, the energy distribution will be

narrower than in the defect-free state. The data are interpreted the way they are in the angular correlation technique.

Doppler shift measurements are faster and more efficient than the angular correlation measurements. The major problems associated with this technique are the limited energy resolution and the electronic stability.

5. Quenching

The process of the quenching method is to heat a sample to a high temperature, referred to as the quench temperature. The sample is then allowed to come to equilibrium, and is finally cooled down in a way that permits the retention of the high temperature vacancy concentration. The goal is to retain the equilibrium concentration in an unperturbed state.

In the past, two different methods have been used to heat the sample. In the first one, the sample was heated directly by passing a current through it. The quench was carried out by lowering the sample into a chilled liquid bath. This method allows a fast quenching rate and the quench temperature can be evaluated from the resistance of the sample. However, the temperature of the sample might not be uniform and small deformation during quench might occur.

In the second method the sample was heated in a furnace and then dropped into a quenching bath. Even though the temperature of the sample is more uniform in the furnace, the quenching temperature is not accurately known because the sample cools down

before reaching the quench bath and deformation may also occur.

Various experimental techniques are available for the measurement of the concentration of vacancies retained in quenched samples. The most widely used are field ion microscopy and resistometry.

5.1 Field Ion Microscopy

The field ion microscopy technique has the advantage over other techniques in that it is the only method capable of observing individual defects at the atomic level and discriminating between the different types of defects by displaying the atomic structure of the sample.

The field ion microscope consists of a small hemispherical metal tip located in a chamber that contains a trace of a gas, such as helium or neon, and a fluorescent screen a few centimeters from the tip where the sample is mounted. The tip is positively charged to a high voltage. The image is formed when the gas ions, ionized by the metal ions released from the tip, are accelerated by the high voltage and hit the fluorescent screen. Interstitials are made visible as bright spots and vacancies as dark spots.

The technique consists of removing in a controlled manner by evaporation an atomic layer, imaging the revealed surface and repeating the cycle. Muller (1959) was the first to use this technique to study quenched-in vacancies in platinum. He found, near the melting point, a vacancy concentration of $5.9\ 10^{-4}$ by

direct counting.

This technique is not without drawbacks. There is the problem of occurence of artifacts that might be interpreted as point defects. Local stress arising from the high potential required for imaging might alter the configuration so that results might not be typical of the bulk material. Ambiguities can arise in distinguishing between different defects, for example between interstitials and impurities.

5.2. Resistometry

Electrical resistivity techniques in quenched samples have been widely used because of the high sensitivity of this property to vacancies and the convenience of its measurements.

Since vacancies disturb the periodicity of the lattice they produce perturbations that scatter the electrons and thus increase the electrical resistivity of the sample. According to Matthiessen's rule, the total resistivity can be presented as the sum of a temperature dependent lattice resistivity, $\rho_0(T)$, and a vacancy contribution resistivity, or quenched-in vacancy resistivity, ρ_v :

$$\rho = \rho_0(T) + \rho_v \qquad (8)$$

ρ_v depends on the concentration of vacancies. Since the concentration is small then ρ_v is small, and at ambient temperature the total resistivity is dominated by the lattice resistivity which is due mainly to phonon scattering. At liquid helium temperature the phonon resistivity is negligible except in the case of

palladium. Thus, the resistivity is due only to quenched-in vacancies, impurities, dislocations and other structural defects including surfaces. Thus the low temperature electrical resistivity method is a powerful tool for the investigation of vacancies. The widely used procedure consists in measuring the low temperature resistivity of the sample in the quenched state and again after an annealing treatment. The difference in these resistivities gives the quenched-in vacancy resistivity, assuming the contribution of other defects does not change.

At low vacancy concentration, it is not unreasonable to assume that the quenched-in resistivity is proportional to the concentration of vacancies, provided that there is no clustering. In this case one assumes that

$$\rho_v = \rho_i \, C_v \qquad (9)$$

where is the resistivity of a unit concentration of single vacancies. This quantity is typically of the order of 2 μΩ cm/atomic%. If a sample could be cooled fast enough to trap-in unperturbed all the vacancies initially present at the quench temperature T, then from equation (5) and equation (9) the quenched-in resistivity will given by

$$\rho_v = \exp(S_f/k - E_f/kT)$$

$$\rho_v = A \exp(-E_f/kT) \qquad (10)$$

The energy of formation of vacancies can be deduced from the

variation of the residual resistivity of the quenched sample with the quenching temperature T. The energy of formation is obtained from the slope of the Arrhenius plot.

One of the major drawbacks of this method is that it is completely non-selective, i.e., all defects contribute to the increase in resistivity. In our discussion we assumed no deviation from Matthiessen's rule. Unfortunately, this deviation could be appreciable even at liquid nitrogen temperature and this will create a discrepancy in the evaluation of the vacancy contribution resistivity. However, at liquid helium temperature, this deviation is negligible.

The success of the electrical resistivity measurements depends on the success of the quenching method. Ideally, it is desired to retain the entire equilibrium concentration of vacancies in an unperturbed state. Since single vacancies have the smallest energy of formation, they will be the dominant quenched-in defect. In general the high temperature structure is not preserved. The quenched structure is affected by factors such as the cooling rate, thermal stress, dislocation density and concentration of impurities. Changes in the vacancy concentration can occur due to the clustering of vacancies, loss of vacancies to sinks, such as dislocations, and generation of additional defects, such as vacancies and dislocations, by plastic deformations caused by thermal stress. In the following we will discuss these disturbing effects.

5.2.1. Vacancy Clusters

Vacancies have lattice strain associated with them, since neighboring atoms relax toward the vacant site. From classical elasticity theory it can be shown that if two centers of strain are adjacent, the total strain energy is reduced. As a result, a certain fraction of vacancies will aggregate to form clusters of varying degree. Cluster distributions and sizes depend on the nature of the metal and the way the vacancies are introduced (Balluffi et al 1970). Vacancy supersaturation, thermal stress and stacking fault energy play an important role in cluster formation (Eyre et al 1977). The ease of formation of clusters depends on the binding energy. It is impossible to avoid clustering in a metal where the cluster possesses a significant binding energy.

For most metals studied to date, the ensemble of vacancy defects present under equilibrium conditions can be adequately described by a system of single vacancies, divacancies and trivacancies (Siegel 1978). In platinum it was found (Berger et al. 1973) that the ensemble of vacancy defects consists mainly of single vacancies and divacancies with the single vacancies being the dominant vacancy defect. Divacancy binding energies and fraction of divacancies near the melting point of some fcc metals are reported in Table 1.2. Of the metals studied, the results show that platinum is the least susceptible to clustering.

The presence of clusters may affect the experimental results. Clustering may increase the vacancy loss during quench

Table 1.2 : Binding energies and fraction melting point of divacancies in fcc metals

Metal	Eb_{2v}	Fraction of divacancies	Method	Reference
Au	0.23	23 %	PA	Dlubek et al (1977)
Al	0.25	43 %	QR	Seeger and Mehrer(1970)
Cu	0.20	10 %	PA	Dlubek et al (1977)
Ni	0.30	23 %	QR	Seeger and Mehrer(1970)
Pt	.11-.19	-	QR	Schumacher et al (1968)
	0.23*	(6 $\pm$ 2) %	FIM	Berger et al (1973)

* Free energy

PA: Positron annihilation

QR: Quenching (resistance measurement)

FIM: Field ion microscopy

if the vacancy clusters are more mobile than single vacancies. Even though the resistivity associated with divacancies is different by no more than a few percent from the resistivity of two single vacancies, the experimentally measured quenched-in resistivity will not accurately reflect the vacancy concentration if the number of vacancy clusters present is a significant fraction of the total concentration of vacancies. Theoretical calculations in the noble metals by Seeger (1962) and Flynn (1962) have shown that the formation of a divacancy from two single vacancies leads to a reduction of the resistivity by at most 10 %.

Assuming that we have only single vacancies and divacancies, the equilibrium concentration of vacancies and the effective energy of formation (i.e. the slope of the Arrhenius plot of $\ln(C_V)$ versus $1/kT$) for an fcc lattice are given by (Seeger 1973):

$$C_V = \exp(S_f/k - E_f/kT)[1 + B]$$

$$E^{ef}_f = E_f + (E_f - E^{b}_{2v})B/(1 + B)$$

where

$$B = 12\exp((S_f - S^{b}_{2v})/k - (E_f - E^{b}_{2v})/kT)$$

E_f and S_f are respectively the energy and the entropy of formation of a single vacancy, and E^{b}_{2v} and S^{b}_{2v} the binding energy and the binding entropy of a divacancy. The above two equations suggest that the Arrhenius plot of the quenched-in resistivity as function of the inverse of the absolute quench temperature will not yield a straight line and the energy of formation is tempera-

ture dependent.

In platinum, Berger et al (1971) have found S^b_{2v} = 1.95k for E^b_{2v} = 0.11 eV. Using these values along with E_f = 1.30 eV and S_f = 0.6k, we have found an upward bending of the Arrhenius plot. This bending has reached 0.4 % at the melting point and has affected the energy of formation by 0.3 % at that point.

5.2.2. Impurity-Vacancy Interaction

Impurities could significantly affect the quenched equilibrium concentration in a number of ways, depending upon the type of impurities involved and their concentration. If the binding energy between a vacancy and an impurity is positive, a certain fraction of the concentration of vacancies is expected to be bound to impurities, increasing the total vacancy concentration. In particular, when the concentration of impurities is comparable to the concentration of vacancies, a sizable fraction of the vacancies that would have reached sinks during quench may be retained in the lattice by impurities. The effect of impurities is more important at low quench temperature (Cotterill and Segal 1963). With increasing temperature the effect decreases since the entropy of mixing which favors the dispersion of impurities becomes more important. Quenching of platinum by Emrick (1978) and Jackson (1965) have shown that, at low temperature, the quenched-in resistivity is larger in lower purity material .

If we assume that binding occurs only when a vacancy occupies a nearest neighbor site to an impurity, the equilibrium

quenched-in resistivity of a low purity sample is given by (Burke 1972):

$$\rho_v = A \exp(-E_f/kT) \left[1-12\, C_s + 12\, \frac{\rho_{is}}{\rho_i} C_s \exp\left(E^b_{sv}/kT\right)\right]$$

where A: entropy factor

C_s: impurity concentration

Eb_{sv}: vacancy-impurity binding energy

E_f: energy of formation of single vacancies

ρ_i : resistivity of a unit concentration of single vacancies.

ρ_{is} : resistivity of a unit concentration of vacancy-impurity complex.

The above relation implies that the Arrhenius plot is in general not linear and the energy of formation is temperature dependent. The energy of formation determined in lower purity samples is lower than the one determined in higher purity samples.

Finally, the impurity might move in and out of solution during quenching and annealing, causing further perturbations in the experimental results.

5.2.3. Quenching Strains

Fast quenched samples are usually strained during quenching. Strains are of two kinds: thermal and hydrodynamic. Thermal strains arise from the temperature gradient, during the quench, between the cool surface and the warm core of the sample. Fast

cooling rates lead to large strains. The generation of hydrodynamic strains depends upon the quenching medium. They are larger in liquids or high velocity gas jets. They arise from the viscous drag on the sample as it moves through the quenching medium.

The effects of strains have been investigated extensively by Takamura (1961,1963) and Jackson (1963,1965). Straining during quench leads to the plastic deformation of the sample and can result in the following effects:

1. Generation of extra vacancies, though they represent a small fraction of the total concentration of vacancies except in thin samples liquid quenched from low temperatures.

2. Production of extra dislocations. An upper limit of the dislocation density generated in gold by a quenching strain of 10^{-3} has been estimated to be of the order of 4×10^{7} cm/cm^3 (Balluffi et al 1970) The extra dislocations act as sinks for vacancies and thus increase the loss of vacancies during quench. Measurements on platinum by Jackson (1963) have shown that quenching strains greater than 10^{-3} produce enough dislocations to absorb a significant fraction of the vacancies present.

The quenching strains thus greatly affect the experimental results. Unless the magnitude and the effect of such strains were known, it would be impossible to relate the experimental data to the concentration of vacancies. Investigation by

Takamura (1963) has shown that the value of the energy of formation of vacancies is reduced by quenching strains. Altough this results has been questioned, the possible influences ofthe quenching strains can be made negligible by the proper choice of the quench rate and the quench medium.

5.2.4. Vacancy Loss

Because of the high mobility of vacancies in metals at temperatures close to the melting point a significant fraction of the equilibrium vacancy concentration is usually lost to sinks in samples quenched in most liquid quench media. These losses, in general, increase with increasing quench temperatures and decreasing quench rates. If such losses occur and are not properly accounted for, they could lead to erroneous values for the energy of formation of the vacancies.

Quenching at different rates and then extrapolating to infinite quenching rate the quenched-in vacancy resistivity values (Flynn et al. 1965, Balluffi et al. 1970, Zetts and Bass 1975) is a possible way to properly correct for such losses. Unfortunately such a technique is not without problems and can yield misleading results (Seeger and Mehrer 1968).

Another approach to this problem has been developed by Flynn et al. (1965) who have solved the vacancy diffusion equation for the case of single vacancies migrating to fixed sinks. Using their results for gold quenched at different rates, they have confirmed experimentaly their theoretical prediction. They have

shown that the fractional loss of vacancies during linear quench is a function which depends only on the product $D_q T_q \tau_q$, where D_q is the vacancy diffusion coefficient at the quench temperature T_q, and τ_q is the time required for the quench.

A more rigorous evaluation of the actual fractional losses of vacancies is estimated by direct numerical integration (Seidman and Balluffi 1965,Polak 1974,Emrick 1978) of the time dependent defect diffusion equation (Carslaw and Jaeger 1947) with time dependent boundary conditions. Sinks of different shapes and distributions have been proposed. Seidman and Balluffi (1965,1966,1967) used a model of regular array of static dislocations of outer radius $R = 1/2\sqrt{N_d}$, where N_d is the dislocation density. Emrick (1978) has extended the calculations to include random and regular arrays of parallel dislocation lines and spherical surface sinks.

These models calculations are based on the assumptions that during quench :

1. The dislocations act as perfect sinks, i.e, maintain the instantenous thermal equilibrium concentration at the dislocation core.
2. The dislocation density is constant.
3. Clustering is negligible.

Seidman and Balluffi (1966) have estimated the efficiency of the dislocations as sinks by calculating the maximum expected losses to the measured density dislocations in gold on the basis of a model in which the rate limiting step is the diffusion of

vacancies from the dislocation lines. Their conclusion is that the efficiency is very high under conditions of moderate to strong defect supersaturation. In general the assumption that the dislocation density is constant is a poor one. Rapid quenching can produce strains large enough to increase the dislocation density. In systems where clustering is significant, cluster diffusion to sinks could be important and would have to be taken into consideration (Flynn 1964).

6. Present Work

The goal of this experiment is to determine a more accurate value of the formation energy of vacancies by drastically reducing the vacancy losses that occur at high temperature during quench by the use of a low dislocation density sample .

Controversy has developed over the values of the energy of formation of vacancies. In platinum these values spread over an interval ranging from 1.15 eV to 1.60 eV. This controversy arises from the difficulty in correct control of experimental conditions such as purity of the material, dislocation content, quenching speeds, and temperature. This controversy arises also from the difficulty of untangling the complicated interactions between defects when several are present.

The major perturbing effects that distort the results are the loss of vacancies to sinks, especially to dislocations, and the thermal strain during the quench. The bulk of the previous quenching experiments have been carried out on long, small

diameter (0.08mm to 0.4 mm) polycrystalline samples. Because of the large surface to volume ratio, handling the sample introduces dislocations with densities in excess of 10^6 cm/cm^3. Detailed investigation has shown that dislocations act as the main sinks for vacancies and therefore are responsible for the vacancy loss. In most previous experiments a high quenching rate has been used to prevent vacancy loss. However, rapid quenching strains the sample, leaving it with a large dislocation density even if most the vacancies are trapped.

The experiment was designed to provide a better control of the parameters that affect the quenching results. The experimental steps taken to remedy for these perturbing effects are:

1. The use of very low dislocation density single crystals. Emrick's calculations (1976,1978) showed that with dislocation density as low as 2000 cm/cm^3, vacancy losses are less than 1 % of the equilibrium vacancy concentration in gold from 950°C at a quench rate as low as 200°C/sec. Lengler (1976) was successful in quenching 1 mm single crystal of gold with low dislocation density with negligible loss of vacancies up to 950 $^{\circ}$C .

2. The use of lower quenching rates to avoid thermal strains. Emrick (1978) calculated vacancy losses during quench of low dislocation density crystals at a variety of quench rates. These calculations showed that vacancy losses of only a few percent would occur for cooling rate as low as a few hundreds of degrees per second. Lengler quenched his samples into a -70°C sulphuric acid solution. Even though most vacancies were trapped, quenching

strains associated with his technique left a large dislocation density in the crystals (Lengler 1977). His subsequent de Has-vanAlphen measurements contained significant contributions from both types of defects. The present experiment offer the possibility of preparing samples with the same equilibrium concentration but low dislocation density so that vacancy-only properties can be studied.

3. The use of a large diameter sample and the use of air as a quenching medium to avoid hydrodynamic strains. Investigations by Jackson (1965) have shown that hydrodynamic strains are reduced by the use of large diameter samples. Air quenching offers the possibility of obtaining low quenching rates. It also eliminates the possibility of hydrodynamic strain and contamination during quench.

4. The use of high purity samples to avoid impurity-vacancy complexes which change the equilibrium concentration.

5. The growth of the sample after each quench to avoid the problem of dislocations introduced by handling the sample. It also assures the use of a fresh sample after each run.

Furthermore, since there is no dislocation production while the quench is in progress, the results could be used to test the validity of the model calculations proposed by Emrick (1978).

For this study, platinum has been chosen. It can be purified by zone refining in air. It does not oxidize and it is not an absorber of gases. The quenched state is stable at room temperature. The vacancy clustering is relatively unimportant.

Direct observation of the equilibrium vacancy population by Berger et al. (1973) has shown that clusters exist only as divacancies and the ratio of divacancies to single vacancies is only 6 %. Platinum has a relatively large equilibrium vacancy concentration at the melting point, so measurable concentrations can be observed over a wide temperature range. In addition, there is a vast store of data for making comparisons.

The major problem we have with platinum is that at present we are unable to characterize the dislocation density by independent measurements. We have been unable to locate an etching procedure for revealing dislocations in platinum and do not have the facilities for transmission electron microscope measurements.

Palladium is one of the remaining unstudied metals which can be done easily by this technique. The results in platinum have been successful. We have been able to eliminate the quench losses. These situations have raised our interest in palladium, so this new method seemed to be appropriate to try on this metal. Moreover, the energy of formation of vacancies in palladium has been measured by the positron annihilation method, so a comparison is possible. Because of our experimental method, the need for an adequate resistance versus temperature scale to near the melting point was required. We have carried out measurements of a high purity palladium single crystal to within 100^{o}C of the melting point. Previous measurements have been done using large size, low purity polycrystalline samples (Laubitz and Matsumura 1972) or uncharacterized samples (Guntherodt et al. 1975) or

lacked sufficient precision in the presentation of the results (Dupree et al. 1975). In contrast, our sample has been a small single crystal, with purity at least 80 times higher than that of the earlier works.

There has been growing interest in the electronic properties of the transition metals, both from a theoretical and from an experimental standpoint (Evans et al. 1971, Mott 1972, Esposito et al. 1978, Dupree et al. 1975 , Van Zytveld 1980). In this study, we measured the molten palladium resistance and compared it to earlier published values.

CHAPTER II

EXPERIMENTAL PROCEDURE

1. Introduction

The experimental procedure used in this investigation consisted of the following steps, to be described in detail subsequently:

1. Purification and growth of a single crystal sample by repeatedly zone refining in air. The sample is grown after each run to provide a fresh new sample and its purity, as measured by the residual resistivity ratio, checked to assure that the sample has not been contaminated.
2. Quenching of the sample, followed by a measurement of the quenched-in resistance increment. The quenching was carried out in two different furnaces, a Metal Research furnace operated with the open end downward and a Lepel rf furnace. Water and air were used as quenching media in quenches carried out in the Metal Research furnace, while in the Lepel rf furnace only air was used.
3. Annealing of the sample in an electrical furnace, followed by a measurement of the vacancy free resistance.
4. X-ray analysis of the quality of the sample.

The need for a temperature scale to determine the palladium quench temperature arose, so measurements of a high purity

palladium single crystal were carried out to within 100 ^{o}C of the melting point. For platinum this calibration was furnished by the supplier and reported in the literature. Due to the interest in the electronic properties of the liquid transition metals (ten Bosh and Benneman 1975), the molten palladium resistance was also measured.

2. Sample Preparation

The starting material for platinum samples were hard drawn 99.999 % 1mm diameter wires obtained from Sigmund Cohn, Inc. According to a certificate of analysis provided by the supplier, detectable metallic impurities were 3 ppm Cu, 2 ppm Pd and 1 ppm Rh. The potential leads were made of 0.08 mm reference grade Sigmund Cohn, Inc., platinum wires.

For palladium the starting material was obtained from Johnson, Matthey and Co., London, in the form of 1 mm diameter rods, 99.999 % nominal purity. According to spectroscopic analysis furnished by the supplier, the metallic impurities present were Fe (4 ppm), Si (2 ppm), Ca (1 ppm) and Cu, Ag and Mg each less than 1 ppm. The fine wire used as potential leads were cut from a 1 mm rod palladium that had been rolled into a 0.08 mm thick sheet.

All wires were first etched in aqua regia and then washed in distilled water. To attain a higher purity the samples were further zone refined in air (Sandesara and Vuillemin 1977).

3. Single Crystal Growth

The essential parts of the zone melting apparatus are shown in Figure 2.1. The molten zone was generated by the rf alternating current induced in a vertically supported sample . The high frequency alternating current required was generated by a 450 KHz, 10 Kw Lepel induction heating generator. The load coil consisted of a ten turn coil of water cooled 1/4 inch copper tubing. Inside the load coil, there was a water cooled eddy current concentrator made of copper. The concentrator permitted a more efficient power transfer and narrower molten zone. A Research Specialties Co., model 2471 drive unit was used for a closely controlled motion of the molten zone. The sample was mounted in a fixed position on the carriage of the 2471 unit. The carriage rolled along a pair of chrome plated steel rods. Multipass operations were obtained by a slow sweep down and with a rapid return up of the sample at low rf power. The concentrator was stationary. The sweep speed was adjustable from 0.22 inch/hr to 15 inches/hr and the rapid return speed was adjustable from 2.4 inches/min to 24 inches/min. The technique used was as follows:

1. Generate a molten zone at the lower end of the sample.
2. Sweep sample down slowly at a rate of 1.5 inches/hr. The carriage and the sample travelled downward, while the molten zone travelled upward relative to the sample. An optical pyrometer was used to control the molten zone by manually adjusting the rf power. When the molten zone had achieved its full travel through

Figure 2.1 Zone refining apparatus

A: lever control, raises or lowers the upper end of the sample.
B: movable sample holder.
C: fixed-position, water cooled concentrator.
D: induction coils, 1/4 inch dia. Cu tubing thermally sunk to the concentrator.
E: vertically held sample, the molten zone is held in place by its own surface tension and by the levitation action arising from the repulsion between induced and inducing current.
F: lower sample holder.
G: spring, allows for thermal expansion of sample.
H: base plate, connected to main drive.
I: sweep control, it permits the choice of the speed and direction of sweep.

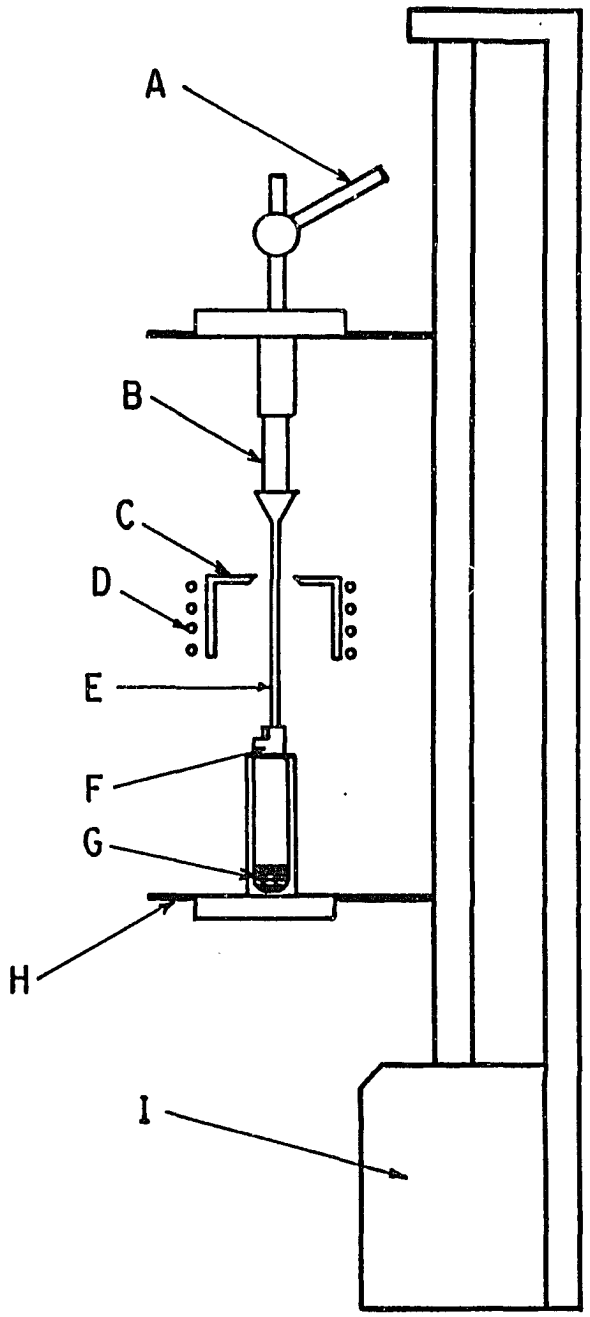

Figure 2.1 Zone refining apparatus

the sample, the motion was reversed, the rapid return activated and the rf power turned down. As the carriage returned to its initial position, the motion was reversed to downward and the slow speed activated. The induction heating generator power was turned up thus generating a molten zone, and the sample travelled downward starting a new pass.

3. Check for purity by measuring the residual resistance ratio, after making an average of fifteen passes.

The above technique was repeated until no noticeable improvement in the purity of the sample was possible. On the average, it took a total of 60 passes to achieve this condition.

The purity of the sample is defined by the residual resistance ratio, which is the ratio of the resistance at room temperature to the size-effect and temperature corrected resistance at helium temperature (see Appendix A). In these high quality crystals, vacancy trapping occurs easily, so resistance measurements intended for purity determinations were carried out on very well annealed samples (as described in section 8 of this chapter). Otherwise, vacancies remaining from the high temperature passes would give an erroneous reading.

The electrical circuit used for the measurement will be described in later this chapter. The measurements were made at room temperature and again without disturbing the current and voltage contacts, while the sample was totally immersed in liquid helium. These measurements were made along different regions of the grown part in an effort to determine the purity gradient

along the sample. Figure 2.2 shows the purity gradient along a palladium sample. The gauge length used for the investigation is taken along the purest part.

The platinum samples had room temperature to helium temperature resistance ratios ranging from 6,000 to 10,000. This corresponded to a residual resistivity ratios between 7300 and 14100. For palladium, the samples had room to helium temperature ratios ranging from 4000 to 13000 corresponding to residual resistivity ratios ranging from 4800 to 27000.

Direct quantitative measurement of the impurity content of the quenched samples was not conducted. However a spectroscopic analysis of a palladium sample by the National Research Council, Canada, is listed in Table 2.1. The sample was taken from the same material used in this study and it had a residual resistivity ratio of 20,000. For platinum, calculations based on the values of the residual resistivity ratio of the samples and the resistivities per atomic percent impurity for the various impurities present in the sample (Blatt 1968, Petroff and Seidman 1971) indicated that the total average impurity content was no higher than $3\ 10^{-5}$ at. fr.

4. Electrical Resistance Measurement

After each quench and each anneal, the resistance of the sample was measured at room temperature and at helium temperature. The sample was mounted in a strain free manner on a holder made of plastic fastened to a 1 m long, 6 mm diameter steel tube.

Figure 2.2 Purity gradient as measured by the residual resitivity, along a palladium sample.

The lower curve represents the ratio of the resistance at room temperature to that at liquid helium temperature. The upper one, the same ratio but corrected for temperature and size effect.

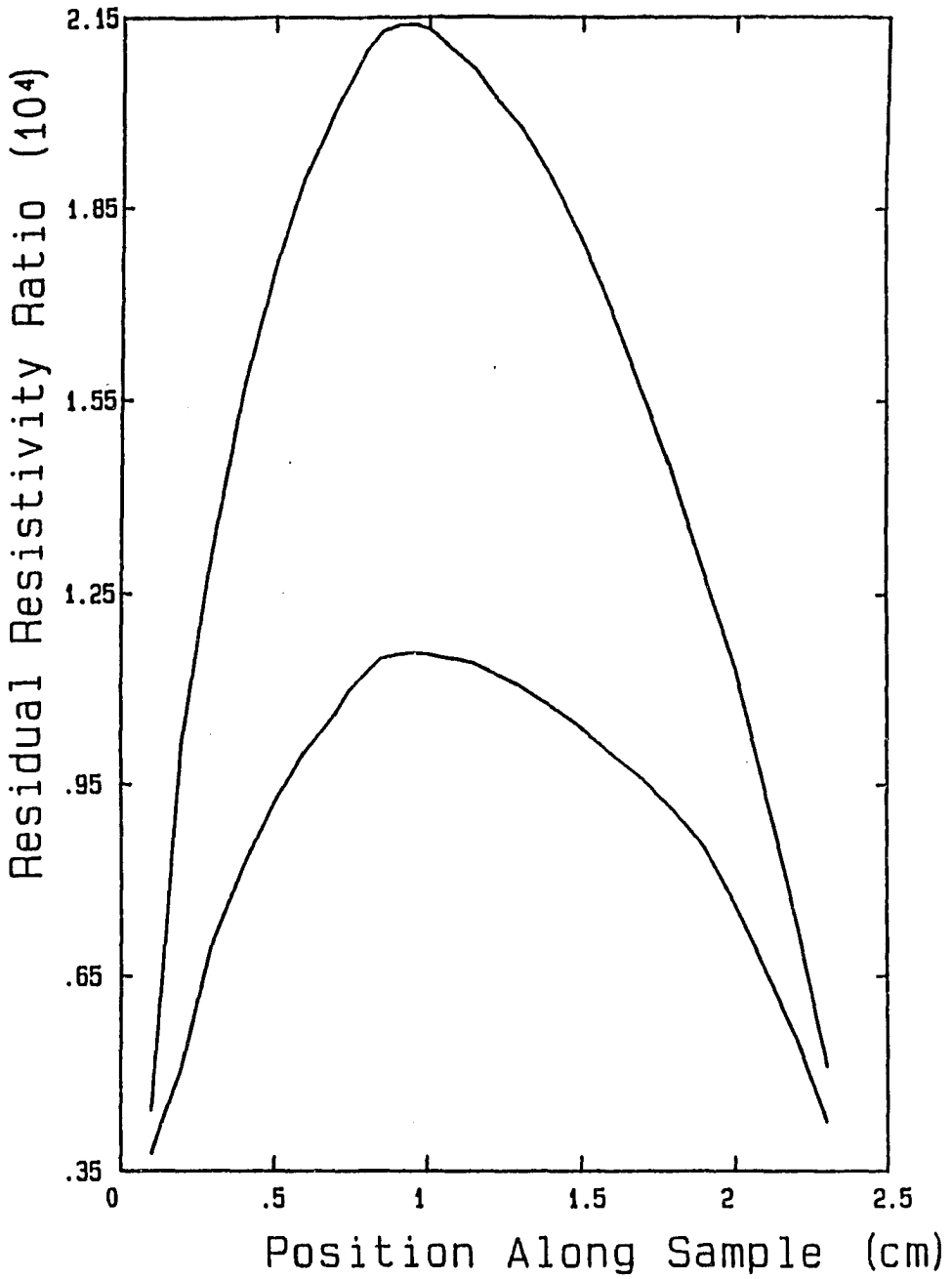

Figure 2.2 Purity gradient as measured by the residual resitivity, along a palladium sample.

Table 2.1: Spectroscopic analysis* of a palladium sample before and after zone refining.

Impurity	Content (ppm atomic)	
	As received	Zone refined
C	100.	20.
N_2	60.	0.6
O_2	20.	3.0
Na	0.1	0.05
Mg	0.6	0.08
Al	3.0	ND
Si	3.0	0.8
P	0.3	ND
S	0.4	0.06
Cl	2.0	0.5
K	0.1	0.1
Ca	1.0	0.01
Fe	5.0	4.0
Ni	0.6	0.6
Cu	0.4	0.3
Zn	0.05	ND
Ga	0.06	0.06
Ge	0.4	ND
As	0.04	0.04
Br	8.	ND
Y	0.05	ND
Nb	0.2	ND
Rh	4.0	0.1
I	1.0	ND
Ba	0.05	ND
La	0.04	ND
Ce	0.3	ND
Ir	0.8	0.08
Pt	3.	0.3
Au	0.3	0.2
Hg	1.0	0.6
Pb	0.2	0.2
W	0.2	ND

*National Rechearch Council, Canada
ND: Non Detectable

The sample was maintained in place by four beryllium copper spring contacts.

In the electrical resistance circuit, a 2 volt Willard low discharge wet cell battery supplied the current, which was varied between 0.25 and 1 ampere by means of a variable resistance. The voltage drop across the sample was measured using a Rubicon 6 dial potentiometer with a 0.01 μV resolution. The current was determined by measuring the voltage drop across a Honeywell 1 Ω standard resistor in series with the sample. The voltage drop across the standard resistor is measured by means of a Fluke digital multimeter to better than 0.1 %. The room temperature was measured to better than 0.5 ^{o}C by means of an ASTM mercury thermometer placed next to the measuring sample gauge.

The helium temperature measurements were carried out using the same circuit and the same method but with the sample holder completely immersed in liquid helium. In order to avoid thermal shock which might affect the defect configuration of the sample, the dipping into liquid helium was exerted very slowly. Since the measuring currents were too low to cause any Joule heating, the temperature of the sample was taken to be 4.2 K. To eliminate the effects of the slowly varying thermal emfs, current reversal was used for both the room temperature and the liquid helium temperature measurements.

The 20^{o}C temperature resistance was evaluated from the room temperature measurements using an available resistance-temperature scale. This resistance was used to normalize the quenched-

in resistance. The qenched-in resistance , ΔR , was taken as the difference between the helium temperature measurements after quench and after anneal.

5. High Purity Palladium Resistance at High Temperature

5.1. Solid Palladium

The crystal was grown over a 4 cm region in the purest part of a 10 cm rod. During the growth of the crystal, the potential leads were grown into the sample 2.5 cm apart. The residual resistivity of the sample used for these measurements was in excess of 25,000.

A small piece of lavite was machined to fit on a four hole 6.25 mm diameter high-grade alumina rod. The sample was then hung by 0.1 mm lead, as shown in Figure 2.3, from the lavite with the potential and the current leads each running through one of the holes of the alumina rod. This lead, used to hang the sample, added a thermal resistance reducing heat loss to the cooler portion of the furnace. The current leads were spot welded to the ends of the palladium rod. The assembly was inserted in a Metal Research PCA 10 furnace capable of reaching a temperature higher than 1700°C. The sample was raised to the uniform temperature region. A 2 volt Willard low discharge battery supplied the current which was varied between 0.10 and 1.0 ampere by means of a variable resistance. The technique was to heat the furnace to a given temperature, let the sample equilibrate for at least 30 minutes, send a small dc current

Figure 2.3 Sample holder used in the MR furnace

C: 0.1 mm dia. current leads.
D: 0.08 mm dia. potential leads.
E: fired lavite.
B: gauge region.
A: vertically held sample.
F: 4-hole, 1/4 inch dia. high grade alumina.

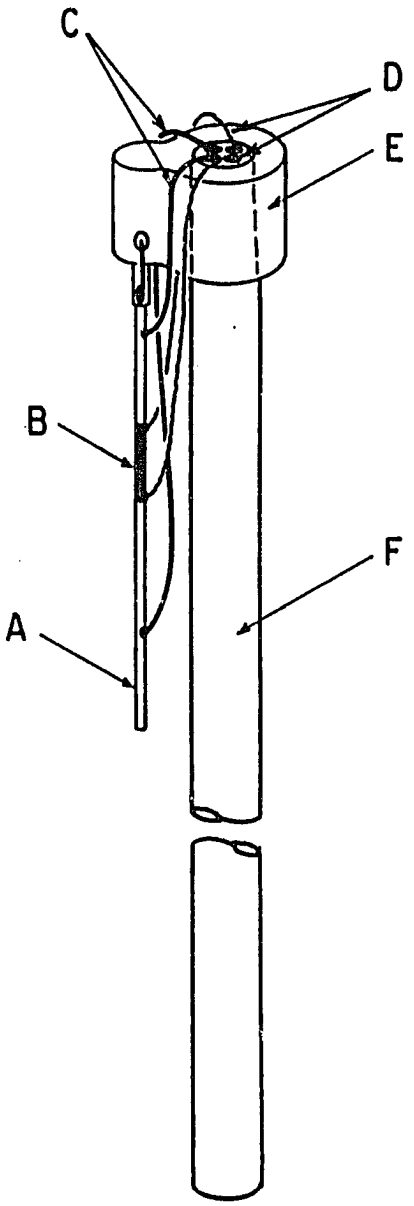

Figure 2.3 Sample holder used in the MR furnace

through the sample and simultaneously measure the voltage drop across the sample using a Leeds and Northrop Co. type K3 Universal potentiometer with a 0.5 μV resolution and the voltage drop across a 1Ω standard resistor in series with the sample using a Fluke digital multimeter. The temperature was measured with a calibrated chromel-alumel thermocouple for temperatures up to 1100°C and a calibrated platinum 6 % rhodium-platinum 30 % rhodium thermocouple for temperatures above 900°C. The thermocouple, placed within 5 mm of the sample gauge region, was monitored using a strip chart recorder and a high precision potentiometer.

The lateral and vertical temperature profiles of the furnace were measured. The vertical gradient of the furnace at 1100 °C is shown in Figure 2.4. The furnace gradient was found to be less than 5 °C over the sample gauge region and the value at midpoint was chosen as the temperature of the sample.

To insure that the sample holder did not electrically short the sample to "ground" or insert parallel resistance between the potential leads at high temperature, measurements of the alumina holder resistance were carried out up to 1650 °C. This resistance was found to be greater than 1 MΩ and thus too large to affect the measured results. The high temperature resistance of the lavite holder was not measured. However open circuit measurements up to 1350 °C showed that the resistance between the potential leads was in excess of 2 MΩ. The sample resistance was 5. mΩ at room temperature.

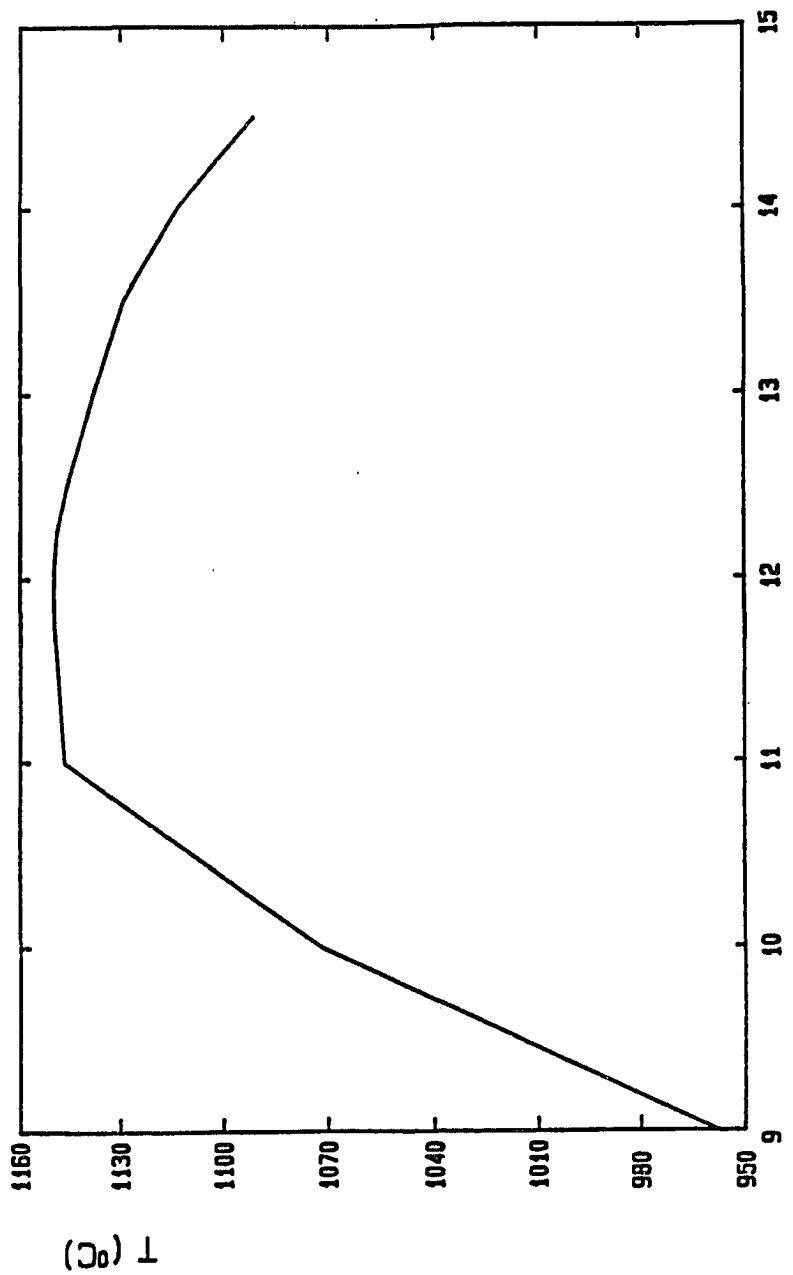

Figure 2.4 Vertical MR furnace gradient at 1100°C

5.2. Liquid Palladium

The measurement of the molten palladium resistance was carried out in the rf furnace used for zone refining. The essential part of the measuring apparatus is shown in Figure 2.5. This method enabled us to do without a crucible and thus greatly reduce the possibility of contamination. The molten zone was held in place by its own surface tension and by the levitation action arising from the repulsion between induced and inducing currents. The sample was mounted with the 0.08 mm wire potential leads already melted in. Using the rf furnace the gauge region was melted and in addition a dc current was passed through the sample. The dc current provided extra heating and a better stabilization of the molten zone, and it permitted the measurement of the electrical resistance.

The resistance was evaluated from the simultaneous measurement, using two Fluke digital multimeters, of the voltage drop across the gauge region and the voltage drop across a calibrated 0.004186 Ω manganin resistor in series with the sample. A rough estimate of the molten zone temperature was given by a disappearing filament optical pyrometer, with the melting actually visually observed through the pyrometer. The sample was cooled and a precise room temperature resistance was measured using a standard four wire dc technique. The room temperature was measured using an ASTM thermometer.

Because of the possibility of the potential leads moving during the melt, special attention was paid to the length of the

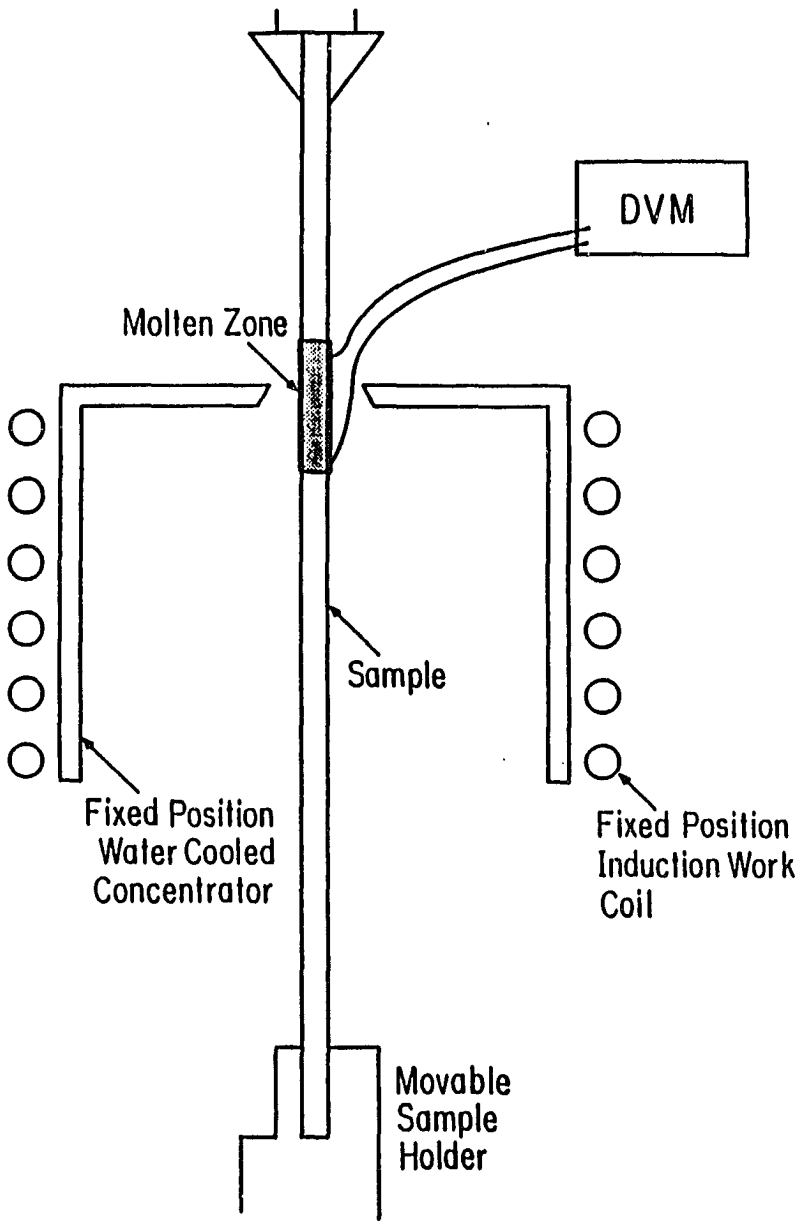

Figure 2.5 Essential part of the molten palladium resistance measurement apparatus.

The sample is held vertically in a movable holder.

sample gauge region. It was measured before and after each run and it was optically monitored through the pyrometer telescope during the run. Motion of the potential leads was cause for the rejection of the run.

To determine the change in the diameter of the sample by melting, an image of the sample gauge region, magnified 31 times by means of a lens, was projected on a photographic print paper before and after freezing. The film was then analysed with a traveling microscope capable of measuring lengths as small as 2.5 10^{-3} mm. The change in diameter was found to be less than 1 %.

6. Quenching Techniques

6.1. Platinum Quench

Prior to the quench, single crystal samples were grown in the rf furnace by the floating zone method from the purified wires. During the growth of the crystal, potential leads of 0.08 mm diameter reference grade wire were grown into the sample 2 cm to 3 cm apart, consistent with good temperature uniformity along the gauge length. Three different methods of quenching were used.

In the first method, a 2 cm to 3 cm long sample was spark cut leaving the fine wire, that has been melted in the sample during growth, at one end as a support. The fine wire was spot welded to a 0.12 mm 99.999 % gold wire which was in turn attached to a support rod. The assembly was raised to a region of an electrically heated furnace where the temperature was uniform. A

styrofoam cup of water with softened paper at the bottom was placed under the furnace in the trajectory of the falling sample. The sample was equilibrated at 1050 ^{o}C for an hour. The temperature was then slowly raised until the gold wire melted, dropping the sample into the water. The quench temperature was assumed to be equal to the melting temperature of gold. After the quench, the sample was dried and then carefully mounted in the 4 terminal resistance measurement sample holder with beryllium copper spring contacts. The room temperature and the helium temperature resistances were then measured.

The second method was a variation of the first one. After the sample had been spark cut, it was mounted on the quenching frame and inserted in a Metal Research PCA 10 furnace as shown in Figure 2.6. The sample was raised to a zero gradient region of the furnace. Quenches were made from temperature up to 1400 $^{\circ}$C . The sample was allowed to equilibrate at the quench temperature for at least one hour. The temperature of the sample was measured by the previously mentioned thermocouples. The junction of the measuring thermocouple was 1 cm or less from the center of the sample and was continously monitored by a strip chart recorder. After the sample had reached the quench temperature and was permitted to equilibrate, the sample frame was allowed to fall from the furnace into a stream of air provided by a diffusion pump cooling fan. After 5 seconds, the sample was placed into a beaker of water. This was done because the ceramic support cooled very slowly and radiation from the furnace might

Figure 2.6 Quenching apparatus in MR furnace.

A: uniform temperature zone.
B: MR furnace.
C: 4-hole, 1/4 inch high grade alumina (sample holder).
D: 4-hole, 1/4 inch high grade alumina (thermocouples holder).
E: moving sample holder (in fully up position).
F: detent.
G: furnace stand.
H: sample-holder frame. The rods are not parallel so that falling holder stops slowly.

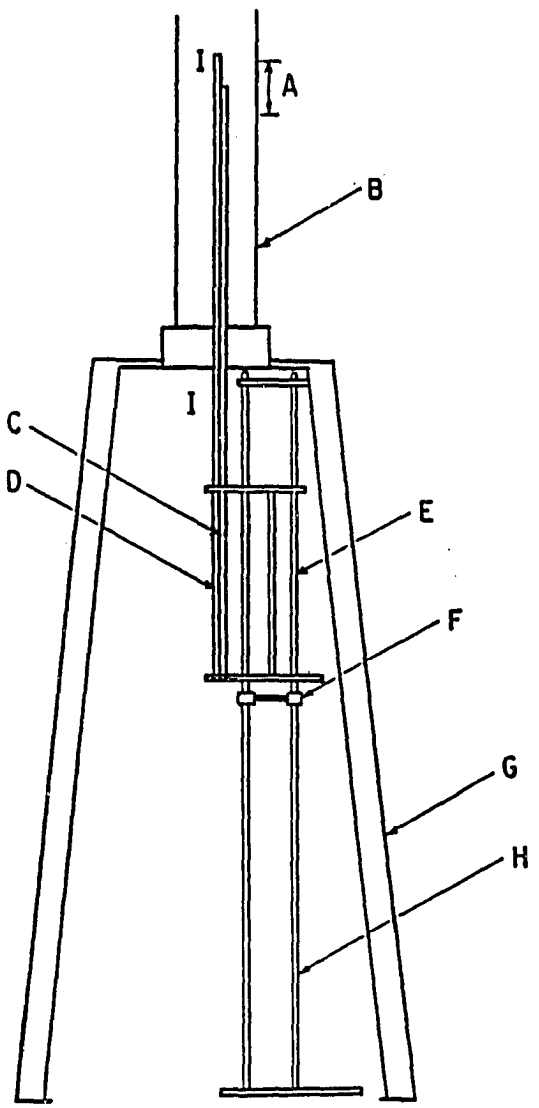

Figure 2.6 Quenching apparatus in MR furnace.

had prevented the sample from cooling below the vacancy annealing peak temperature. After the quench, the sample was dried and its resistances at room temperature and helium temperature were measured.

In the third method, in order to reduce sample handling to a minimum and therefore eliminate the possibilty of contamination and the possibility of increasing the dislocation density, the quenching was made in the rf furnace. This permitted the availibility of a freshly grown sample at each quench. The quenching apparatus is represent schematically in Figure 2.7. It consisted of three main components:

1. The rf furnace
2. The heating circuit used to heat the sample and determine its temperature from its resistance. It provided also a more uniform Joule heating of the sample and a stabilisation of the molten zone during the growth of the crystal. By means of a Tyron Electronics power supply, a dc current of up to 20 amperes was passed through the sample and through a calibrated high current manganin resistor in series. The sample temperature was determined from the measurement of the gauge region resistance and the use of the resistance versus temperature scale that will be described later.
3. The baffle circuit. It was used to hold a baffle in front of of the fan providing the air stream to quench the sample, so that no moving air reached the sample before quench. The baffle was held by a solenoid which was activated when a sensor detected a

Figure 2.7 Schematic representation of the RF furnace quench apparatus.

a: sample.
b: fixed-position, water cooled concentrator
c: induction coils, 1/4 inch dia. Cu tubing thermally sunk to the concentrator.
d: power supplies
e: relay, controls the RF furnace and the baffle circuit. It is controlled by the heating circuit.
f: coil, a magnitised iron core inside the coil holds the baffle till quenching.
g: baffle, prevents air from reaching the sample until release at quench.
h: Fluke multimeters, used to measure the resistance of the sample.
i: Fan.
r: 0.004186 calibrated manganin resistor.

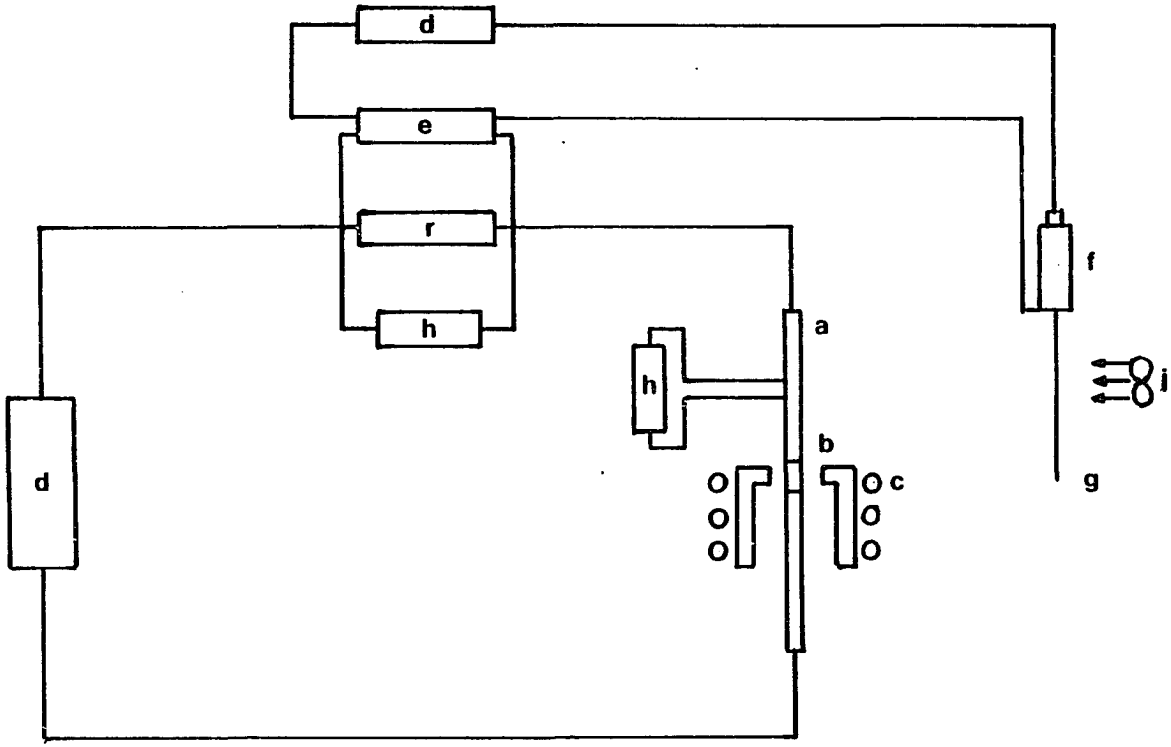

Figure 2.7 Schematic representation of the RF furnace quench apparatus.

current flowing through the sample. A Heathkit regulated power supply was used to provide the current.

The rf furnace and the baffle circuit were controlled by a relay. The relay itself was triggered by the current flowing through the heating circuit. The relay closed at a heating circuit current above 1.5 amperes. In this method, the sample was kept in the rf furnace. After the potential leads were grown in the sample 2 cm to 3 cm apart, a current of 15 to 20 amperes was maintained through the sample while the single crystal was being grown. The molten zone was moved to a point 5 cm to 6 cm below the measuring gauge region. The current was then adjusted until the just-grown sample was at the desired temperature as determined from its resistance. The sample was equilibrated for 10 minutes at this temperature. Using two Fluke digital multimeters, the voltage drop across the gauge length and across the calibrated manganin resistor were visually monitored. The rf power was then increased until the wire below the sample region melted, stopping the heating current. This caused the relay to open, turning off the rf furnace and dropping the baffle allowing the air stream to cool the sample. Just before the quench the voltage across the gauge length and the calibrated manganin resistor were recorded. All the events occuring during the parting of the sample happened nearly simultaneously. A precise room temperature sample resistance measurement was made after the quench using the same electrical resistance measurement circuit. The quench temperature was determined from the resistance versus

temperature calibration curve. The brief increase in rf power to part the sample caused no measurable sample gauge temperature increase.

Because the lower sample mount was a sliding joint, no stress was applied to the sample due to the thermal length changes as the sample temperature was changed during crystal growth and while the quench temperature was being reached. Since the sample parted at quench only the low sample inertia would be responsible for strains, so that the quench is essentially strain-free.

After quenching, the sample was taken out of the rf furnace and mounted carefully in the electrical resistance measurement holder, and room temperature and liquid helium temperature measurements were made. In this case the potential leads were used for the voltage measurements and the beryllium copper spring contacts for the current flow only.

6.2. Palladium Quench

All the palladium quenches were carried out in the rf furnace. The same set up used to quench platinum in the rf furnace was used here. In the first quenches, due to the lack of an adequate temperature scale, the quench temperature was measured within 25 ^{o}C with a disappearing filament optical pyrometer. The quenched-in resistance was estimated from the difference between the inverse of the residual resistivity ratios before and after annealling. The subsequent quenches were

carried out exactly the way they were carried out for platinum quenched in the rf furnace.

7. Quench Temperature Determination

7.1. Thermocouple Calibration

The calibration of the platinum 6% rhodium-platinum 30 % rhodium was supplied by the manufacturer. It was compared with the chromel-alumel thermocouple using standard tables and the two thermocouples agreed within 3°C. The two thermocouples were further calibrated, in our laboratory, using the known melting points of gold, silver and copper. The calibration was carried out by placing a short piece of high grade fine wire of one of the mentioned metals near the thermocouple. This piece of wire formed part of a dc circuit arranged so that the melting of the wire was recorded as the furnace was slowly warmed through the melting point. Agreement between the temperature calibration furnished with the thermocouple and the melting point of the wire was within 2°C. New thermocouple junctions were made every three or four quenches to avoid the problem of junction diffusion.

6.2. Resistance Versus Temperature Calibration

In the case of platinum, the quench temperature was determined from a resistance-temperature scale furnished by the manufacturer. The temperature scale was of the form

$R(T) = R (1 + \beta T + \alpha T^2)$ where T is the temperature in

celsius, R is the resistance at 0°C, β=0.00397794 / ° C and α=-5.875 10^{-7} / ° C^2.

For palladium, the high temperature measurements of the high purity single crystal resistance were used to determine the quench temperature. The best fit of these measurements was used as a resistance-temperature scale. This scale was of the form:

$$R(T) = R_{22}(A_0 + A_1T + A_2T^2 + A_3T^3)$$

with

$$A_0 = 0.9301$$

$$A_1 = 0.3627\ 10^{-2} / °C$$

$$A = -0.1235\ 10^{-5} / °C2$$

$$A = 0.2039\ 10^{-9} / °C3$$

R(T) being the resistance at temperature T expressed in celsius and R_{22} the resistance at 22°C.

8. Annealing Procedure

To measure the resistance of the vacancy free crystal and thus determine the quenched-in resistance due to vacancies, the sample has to be annealed after each quench. The anneal process permitted the annihilation of all the vacancies introduced during the quench. Annihilation could be accomplished by two different mechanisms, migration to sinks and recombination if interstitials are present (in our case they are not). The annihilation is function of the mobility of vacancies. Since the mobility of vacancies increases with increasing temperature, the sample to be annealed was placed in a high grade alumina crucible and mounted in an electrically heated furnace. The sample was heated to a

temperature that produced the highest mobility of the vacancies without affecting the general structure of the sample. The temperature of the furnace was then decreased very slowly to allow enough time for the vacancies to migrate to sinks or to recombine.

The anneal procedure for platinum was to increase the temperature slowly to 1100°C and let it equilibrate for 4 hours. It was then decreased by 100°C every hour until it reached 400°C. The sample was left overnight at 400 °C, then it was cooled down at a rate of 100 °C every half an hour.

For palladium, the anneal procedure was to heat the sample to 1000 °C and leave it at this temperature for 3 hours. Afterward, it was cooled down at a rate of 100°C every hour until the temperature reached 300°C. At this point, the sample was left at 300°C overnight and subsequently the temperature was decreased by 100°C every half an hour.

After each anneal, the sample was mounted in the electrical resistance circuit four spring contacts holder, and its room temperature and its helium temperature resistances measured. The quenched in resistance due to vacancies was taken as being the difference between the helium temperature resistance after quench and the helium temperature resistance after anneal. Before starting the next quench, the sample was given a cleaning etch in a solution of nitric acid and hydrochloridric acid. This solution should effectively remove impurities introduced on the surface during annealing and handling of the sample.

9. X-ray Analysis

The growth of a crystal from the melt is susceptible to imperfections. Common imperfections include striations which are substructures consisting of columnar regions differing a few degrees from neighbouring ones, and twinning, a situation in which crystals are composed of two or more portions that have certain specific orientations with respect to each other. These imperfections were major problems in quenching since they were acting as sinks. In these cases vacancy losses were very large. These imperfections were revealed by the use of back reflection Laue diffraction. When the incident X-ray beam in a back reflection Laue diffraction happened to straddle a boundary between two imperfect regions of a crystal, the two would be jointly recorded. The back reflection Laue diffraction photography was also used to determine the orientation of the single crystal.

A standard back reflection Laue apparatus was used. A Polaroid XR-7 system for X-ray crystallography with a Polaroid type 57 film (ASA 3000) were used to record the back reflected X-rays. The exposure times were 6-10 minutes and the processing times were 10 seconds. The samples were mounted perpendicular to the incident X-ray beam. The distance between the film and the sample was 3 cm. With the aid of a Greninger chart for reading angular relation and a Wulf net, the precise orientation of the sample was determined from a stereographic projection.

CHAPTER III

RESULTS AND DISCUSSION

1. Platinum Quench

1.1. Preliminary

As stated in the first chapter, results on the properties of point defects in platinum as reported in the literature vary considerably. To reconcile these results many important factors have to be taken into consideration : purity and quality of the samples, quenching and annealing methods, resistance increment measurements and temperature measurements. All these factors affect the outcome of a quench experiment. In most of the reported studies essential details are missing. Table 3.1 is a compilation of all the available essential experimental details along with the energy of formation for a number of previous resitance quenching investigations. Table 3.2 is a compilation for other experimental techniques.

We restate that there is a significant difference between the present experimental procedure and the previous ones. The actual samples are 1 mm diameter low dislocation density single crystals. In all the other experiments, the samples used are polycrystal wires with diameter at best half the size of the samples used here, a dislocation density at least an order of

Table 3.1 Previous Platinum Quenches (resistance measurements)

Sample Diameter (mm)	Prequench Treatment	Purity (RRR)	Quenching Medium	Initial Cooling rate (10^4 C/sec)	Quenching Temperature	Annealing Method	Measuring Temperature (K)	EF (eV)	Reference
0.05 0.1 0.2	Annealed at 1500 C in air	99.999%	Water (4 C)	30	900C-1000C	Anneal at 1200 C with slow cooling	77	1.4 ± .1	Bradshaw, Pearson (1956)
0.04 .07 0.1	Annealed at 1500 C in air	99.999%	Water Air	3 6.2	850C-1690C	Anneal at 700C/hr slow cooling	77	1.23 ± .03	Ascoli et al (1958)
0.04 0.1		99.999%	Water+ Air	3 1	1050C-1690C 1050C-1375C		288	1.20	Bacchella et al (1959)
0.05 0.10		(500)	Water Air		800C-1500C		4.2	1.17 ± .02	Lazarev, Ovcharenko (1959)
0.10	Annealed at 1300 C in vacuum for 1hr	99.9%	Helium		900C-1400C	Anneal at 500C for 8 min.	295	1.43	Kogan (1965)
	Annealed 1700 C/5 min 1000 C/10 min 700 C/1 hr	(3000-5000)	Water	5	700C-1000C		4.2	1.51 ± .04	Jackson (1965)
0.08	Annealed in vacuum	(1800)	Helium	0.7	1000C-1700C	Isochronal anneal 200 C - 500 C	4.2		Schumacher et al (1968)
0.05		(600)	Water Argon	10 0.3 - 0.5	1100C-1500C		293		Rattke et al (1969)
0.10	Annealed 927 C/30 min 1223 C/2 hr	(800-1500)	Helium (-100 C)	1.5	800C-950C	Anneal 500C/4min cool at 170C/min	4.2 77	1.51 ± .04	Inigal, Sizman (1972)
0.07	Annealed in air 1500 C/2 hr	(580)	Helium	7	750C-1430C		4.2	1.47 ± .03	Charles et al (1975)
0.25 0.1 0.4	Annealed in air	(5000-10000)	Water Air	0.03 - 7	700C-1500C		4.2	1.30 ± .05	Zotts, Base (1975)
0.05 0.10	Annealed in air	(2480)	Air, argon Helium	1.8 5 - 28	800C-1200C	Anneal 650C-800C for 10-20 min.	273 4.2	1.31	Nisek (1979)
0.08 1.0	Single crystal	(3000) (100000)	Argon Air, water	0.02	900C-1100C	Anneal at 1100C slow cooling	4.2	1.15 ± .01	Eerick (1982)
1.0	Single crystal	(5000-10000)	Air	0.02	900C-1550C	Anneal at 1100 C slow cooling	4.2	1.30 ± .03	Present work

Table 3.2 Platinum defect study by other method than quenching

Sample Diameter (mm)	Pretreatment	Purity (PPM)	Quenching Medium	Quenching Temperature	Measurement Method	Measuring Temperature	EF (eV)	Reference
0.13		1000-3000	Water (15-17C)	1250-1650C	Thermoelectric Force	20C-150C	1.41 ± 0.04	Gertstriken and Novikov (1964)
0.05		99.99%		1300C-	Magnetic Susceptibility		1.40	Dekhtyar and Nikhalenkov (1960)
0.05					.Resistance .Specific heat	727C-1227C 1427C-1727C	1.60	Kraftmakher and Lanina (1965)
0.2	Cleaned & strain Annealed at 1500 C	(3000)	NaCl-H20 (-5 C)	1700C	.Resistance .FIM	4.2K		Berger et al (1973)
		99.99%			Positron Annihilation		1.32 ± 0.04	Maier et al (1979)

magnitude larger, most of the time with a much lower purity and a quenching rates at least two orders of magnitude larger. In the following, we will present the experimental data and discuss them in light of the new quenching technique.

1.2. Results

Figure 3.1 summarizes our results for platinum. It shows the variation of the resistance quenched-in, normalized to the resistance of the sample at 20 ^{o}C, as function of the inverse absolute quench temperature. Normalization of the quenched-in resistance is used to correct for size changes and permit direct comparison of data for samples of different lengths. We can see that for temperatures above 1300 ^{o}C, there is a considerable vacancy concentration loss for some of the samples. The x-ray pattern of one of the samples with very low quenched-in normalized resistance showed that the sample was striated. Subsequent quenched samples were checked, and it was found that all striated samples give low values of normalized quenched-in resistance. Assuming that all the low value results are from striated samples, we have presented in Figure 3.2 the data for samples whose high quality can be verified. The discussion will be limited to the good quality crystal results. The solid line drawn is a linear regression fit of the data. The linear fitting done to the relation:

$$\Delta R(T)/R_{20} = A \exp(-E_f/kT) \text{ gives}$$

$$E_f = 1.24 \pm 0.02 \text{ eV}$$

Figure 3.1 Summary of all quench data of the platinum single crystal.

Normalized quenched-in resistance as function of the reciprocal absolute quench temperature.

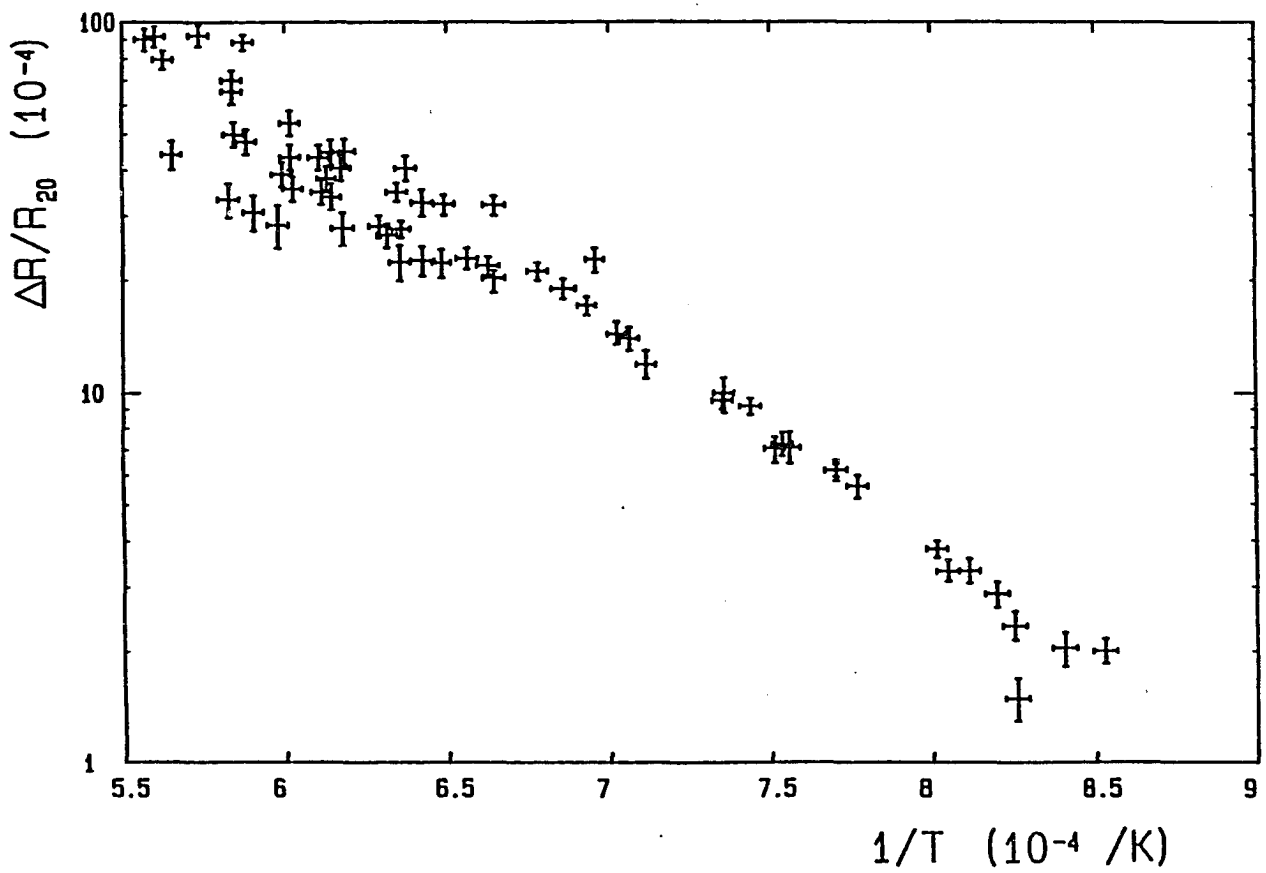

Figure 3.1 Summary of all quench data of the platinum single crystal.

Figure 3.2 Results for striation-free platinum single crystal samples.

Normalized quenched-in resistance as function of the reciprocal absolute quench temperature.

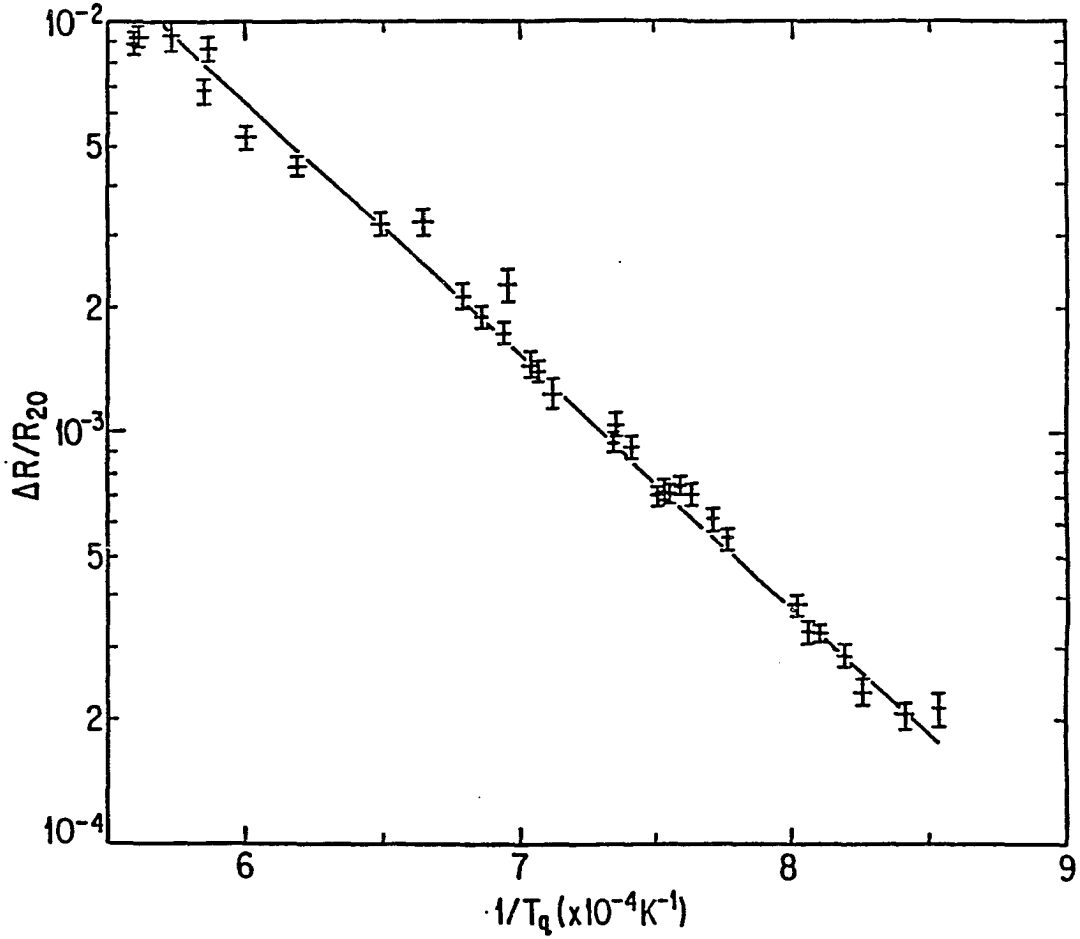

Figure 3.2 Results for striation-free platinum single crystal samples.

$$A = 39 \pm 6$$

$\Delta R(T)$ being the quenched-in resistance at quench temperature T, R_{20} the resistance of the sample at temperature 20 °C and k the Boltzmann constant.

However a least-squares fit to the data for quench temperatures below 1200 °C to the same equation gives

$$E_f = 1.30 \pm 0.03 \text{ eV}$$

$$A = 66 \pm 17$$

The energy of formation is roughly 5 % higher than the one derived from the fit of the whole set of data. As reported in chapter I, the contribution of the divacancies is too small to explain this difference. It is less than 0.12 % up to 1550°C. The most likely explanation of this is that we do have small losses for temperatures above 1200 °C. Extrapolating the low temperature results to higher temperatures, we find losses are about 13 % at 1500 °C and 10 % at 1400 °C. The quenching rates were not measured. However, the air quenching rates under similar circumstances were determined, by direct measurements on 1 mm diameter gold rods, to be 160°C/sec to 300 °C/sec (Emrick 1982).

The dislocation density of our samples can be estimated by using the model calculation proposed by Emrick (1976). This model, reasonably accurate at dislocation densities up to 10^8 cm/cm^3, is a random array of parallel dislocation lines which maintain instantaneous thermal equilibrium. Figure 3.3 shows the model calculations of the vacancy concentration retained at

different quench temperatures as function of the dislocation density for quenching rates from 160 °C/sec to 300 °C/sec. These results imply a dislocation density in our samples in the range 7× 10^5cm/cm^3 to 10^6cm/cm^3. This is in agreement with the preliminary measurements of low angle electron scattering by the de Haas-van Alphen technique using scattering parameters based on copper crystals with known dislocation density (Emrick and Vuillemin 1981, Chang and Higgins 1975).

1.3. Energy of formation

As shown in Table 3.1 and Table 3.2, the energy of formation E_f determined by various authors ranges from 1.15 eV to 1.60 eV. The present value is 1.30 $\pm$ 0.03 eV. This value is in good agreement with the values determined by quenching by Misek (1979) and by positron annihilation by Maier et al (1979). Zetts and Bass (1975) found a similar value by applying the Flynn-Bass-Lazarus theory to their quench results.

However, the present value is larger than the 1.15 eV value reported by Emrick (1982) and much lower than the 1.50 ev reported by Jackson (1965). Even though the starting samples used by Emrick are similar to the ones used in this study, the technique he used leads to the straining of the samples while handling before the quench thus increasing the dislocation density and the vacancy loss. Jackson used high purity polycrystal samples and carried out a careful analysis of the data. However his measurements were made over the small range of 650 °C-

Figure 3.3 Remaining vacancy concentration as function of the dislocation density for quench temperatures between 800°C and 1500°C. The quenching rate is 160°C/sec - 300°C/sec.

The model is single vacancies migrating to a random array of parallel dislocation lines which maintain the instanteneous thermal equilibrium vacancy concentration. E_m=1.38 eV and $\nu = 1\times10^{13}$/sec (similar values were found using E_m = 1.60 eV and $\nu=2\times10^{13}$/ sec)

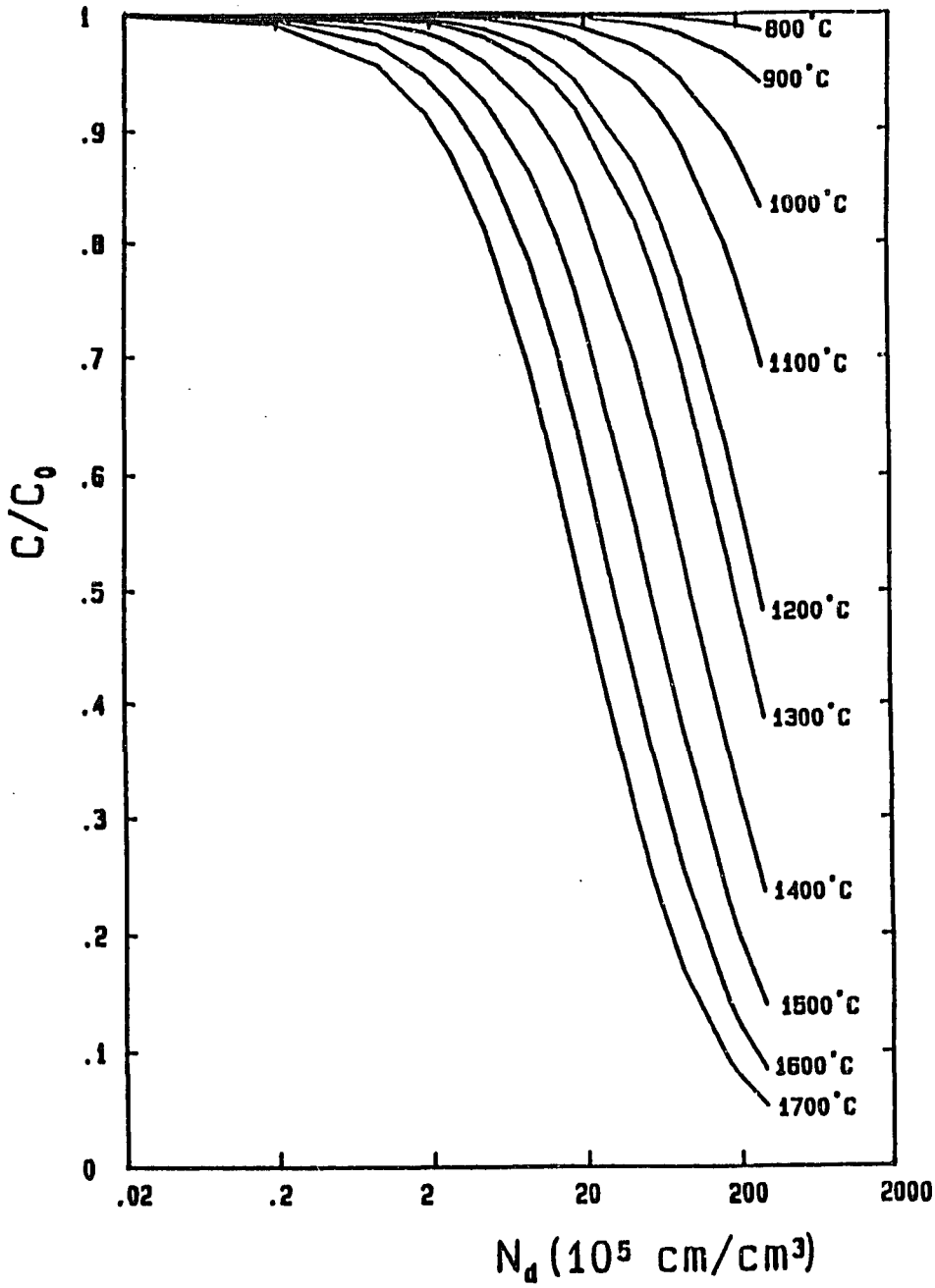

Figure 3.3 Remaining vacancy concentration as function of the dislocation density for quench temperatures between 800°C and 1500°C. The quenching rate is 160°C/sec - 300°C/sec.

900°C. It has been argued (Zetts and Bass 1975, Misek 1979, Emrick 1982) that the large value determined by Jackson, and believed until recently to be the "best value", is due to his assignment of more weight to the low temperature data than can be justified.

1.4. Entropy of formation

Our quench experiment allows us to determine the single vacancy entropy of formation S_f. Using the results of the data fitted up to 1200°C, we have the entropy factor $A = 66 \pm 17$. The resistivity per unit concentration of vacancies has been reported to be equal to 4.6×10^{-4} μΩcm/at.fract. (Schaeffer 1982).

Combining these data and taking the platinum resistivity at room temperature equal to 10.63 μΩcm (converted from the ρ_0 = 9.876 μΩcm of Flynn and O'Hagan 1967), we find that $S_f = (0.42 \pm 0.11)k$. This value is at the low end of the range found for most fcc metals, 0.6k to 2k as reported by Seeger (1976). Our error assignment is statistical only so that the absolute uncertainty is undoubtedly larger.

In addition, with E_f = 1.30eV and the above values, the concentration of vacancies at the melting point, T_m = 1769°C, can be calculated from equation (5) to be $C_V = (9.4 \pm 0.7) \times 10^{-4}$. As shown in Table 3.3, this result is in good agreement with the quenching value reported by Schumacher et al. (1968) and by Zetts and Bass (1975) and the positron annihilation value reported by Shaeffer (1982). However it is much smaller than the dilatometry

Table 3.3 Platinum vacancy concentration at the melting point

$C_v(T_m)$ (10^{-4})	Method	Reference
24	Quenching	Jackson (1965)
26.	Dilatometry	Kopan (1965)
100.	Specific heat	Kraftmakher and Strelkov(1966)
8.4	Quenching	Schumacher et al (1968)
10.	Quenching	Zetts and Bass (1975)
10.2	Positron	Schaeffer (1982)
9.4	Quenching	Present work

value reported by Kopan (1965), the specific heat value reported by Kraftmakher and Strelkov (1966) and the quenching value reported by Zetts and Bass (1975) derived from Jackson's data (1965).

The low values are more likely to be correct due to the better control of the experimental parameters that affect the results. As discussed in chapter I, since the measurements in the dilatometry method involve small differences in large quantities, the uncertainty in the determination of the vacancy concentration could be very large. The same argument can be used for the specific heat measurements. The large value derived from Jackson's data could be due to the extrapolation of the data from 900°C to the melting point.

1.5. Experimental Errors

Neglecting vacancy loss during quench, the experimental accuracy of the quenched data is mainly limited by the uncertainties in the determination of the quench temperatures and the measurements of resistance in liquid helium.

1.5.1. Determination of the quench temperature

1.5.1.1. RF furnace Quench

In the quenches made in the rf furnace, the accuracy with which the sample quench temperature can be determined depends upon:

1. The accuracy in the measurements of the room temperature

and the high temperature resistances.

2. The effect of the rf furnace on the measurements of the high temperature resistance.

3. The uniformity of the temperature distribution along the measuring gauge region.

4. The accuracy of the temperature scale furnished by the material supplier and the effect of purity on it.

Both the room temperature and the high temperature resistances were measured with a precision better than 0.5 %. This introduces an uncertainty of 5 °C in the quench temperature. Possible temperature nonuniformity along the gauge region, due to convective turbulence around the sample, increases the uncertainty to between 7 °C and 13 °C for quench temperatures between 900 °C and 1550 °C.

During the measurement of the palladium resistance at high temperature, we checked the validity of our measurements by reproducing the platinum results. The resistance of a single platinum crystal was measured up to 1600 °C and its temperature monitored by a calibrated platinum 6 % rhodium-platinum 30 % rhodium thermocouple. It was found that the temperature scale provided by the platinum supplier and the thermocouple agreed within 3 °C.

To check the effect of the rf furnace on the measurement, the resistance was measured with and without the rf furnace on. Both an actual sample and a calibrated standard resistor were used. No noticeable effect was found.

1.5.1.2.MR Furnace Quench

For the measurements carried out in the Metal Research (MR) furnace, the precision in the determination of the temperature depends on the accuracy of the thermocouples used and the temperature gradient along the gauge region. The precision and calibration of these thermocouples has already been been discussed. As mentioned in section 2.4 the temperature gradient is not constant but a function of the temperature. It varies between 2 ^{o}C and 5 ^{o}C over the sample gauge region. The possible change in temperature caused by the sample falling through the air before reaching the quenching medium introduces an additional source of error of the order of 10 ^{o}C.

1.5.2. Resistance Measurement in Liquid Helium

The voltage across the sample dipped in liquid helium was measured with a resolution of 0.01 μV. The current was measured with a precision of better than 0.1 %. Typical measuring voltages and currents are of the order of 2 μV and 1 ampere respectively. The uncertainty in the determination of the liquid helium temperature resistance is then 0.01 $\mu\Omega$. This is equivalent to an uncertainty of about 1 % in the normalized quenched-in resistance in platinum at a quench temperature of 1250 ^{o} C.

1.6. Comparison to Early Work

Figure 3.4 shows the present results compared to previous air quench results of some other workers. Since essential details are missing in most of the previous studies, only a

qualitative comparison is possible. In the cases where the quenched-in vacancy concentration is represented by the resistivity ρ and the resistivity is not reported, ρ is converted to the resistance ratio scale $\Delta R/R_{20}$ by using the value of ρ_{20} = 10.67 μΩcm (Flynn and O'Hagan 1967). Figure 3.4 shows that in the present case the linearity of the Arrhenius plot extends over a larger temperature interval than in the previous studies. This is despite the fact that the present quench rates are an order of magnitude smaller than in some of the previous cases.

Figure 3.5 displays the present results along with those of earlier fast quenches. The cooling rates for these fast quenches can be two orders of magnitude larger. Here we can see that the linearity of the Arrhenius plots of these previous quenches do not extend over as a large range of temperature as does the present plot.

In summary, we have been able to quench more vacancies than was done in previous work with the slowest quenching rate possible. We proved that fast quenches are not necessary to trap essentially all the equilibrium vacancy concentration in low dislocation density samples. We introduced a new technique that eliminates the introduction of unwanted dislocations during quench.

1.7. Vacancy Loss,Dislocation Density and Quenching Rates

To show the effect of the dislocation density on the fraction of the equilibrium vacancy concentration quenched in a

Figure 3.4 Comparison with previous slow quench results.

Normalized resistance quenched into platinum air quenched as function of the inverse absolute quench temperature.

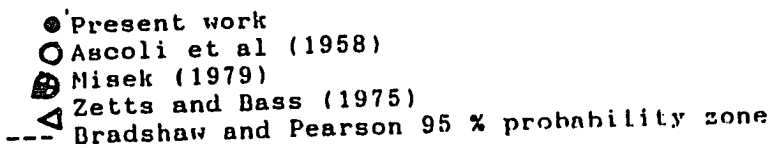

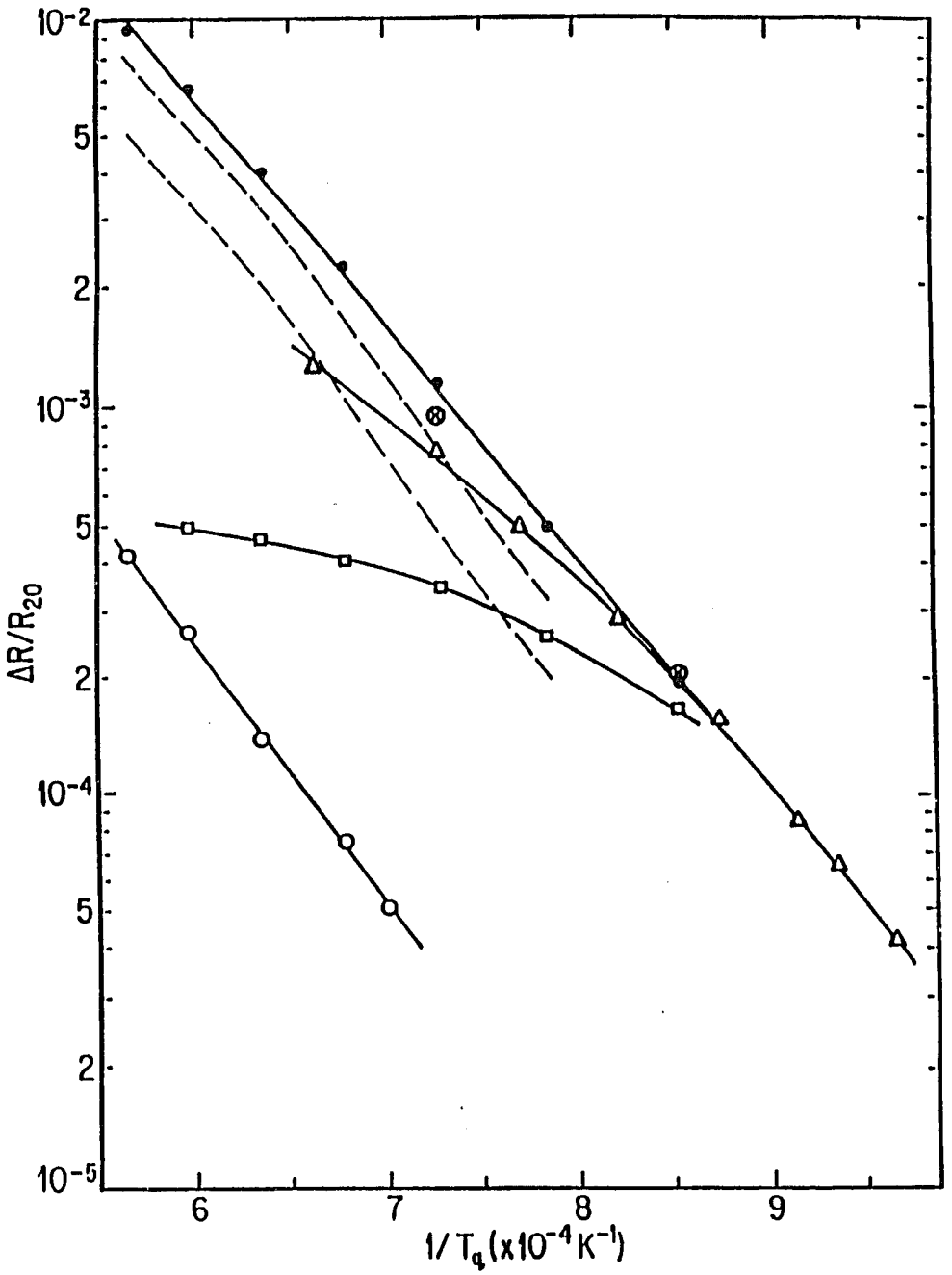

Figure 3.4 Comparison with previous slow quench results.

Figure 3.5 Comparison with previous fast quench results.

Normalized resistance quenched into platinum water quenched as function of the inverse absolute quench temperature.

- Present work
- Zetts and Dass (1975)
- Heigel and Sizman (1972)
- Charles et al (1975)
- Jackson (1965)
- Ascoli et al (1958)
- Bacchella (1959)
- Kopan (1965)
- Rattle (1969)

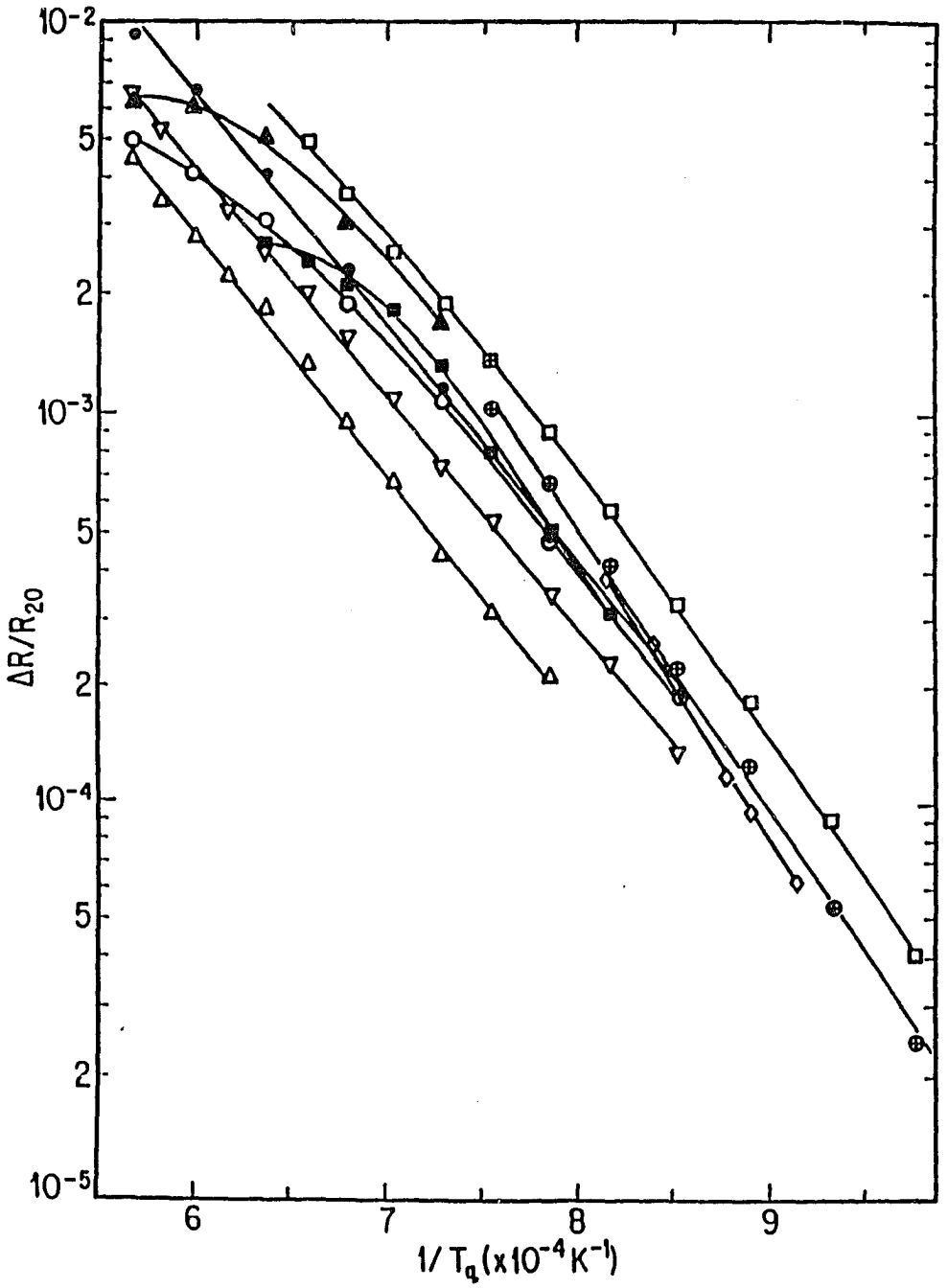

Figure 3.5 Comparison with previous fast quench results.

sample, we compared our results to those of Zetts and Bass(1975) in Figure 3.6. Their polycrystal results have been chosen for comparison because the samples used have a purity, as measured by the residual resistance ratio, comparable to the present samples. Also, to our knowledge, there are no measurements made on large single crystals of platinum using the quenching method. In the subsequent discussion polycrystal results refer to the Zetts and Bass work. Single crystal results refer to the present work.

As shown in Figure 3.6, the main difference between the results obtained in the single crystals and the thinner polycrystals is in the amount of quenched-in resistance above 1000^{o}C and in the linearity of the Arrhenius plot. For the single crystals, the losses of vacancies compared to the polycrystal losses are negligible. The vacancy concentration quenched in the single crystals is insensitive to quenching rates. The water quench values of the single crystals lie within experimental error of its air quenches. In contrast, for the polycrystaline samples, vacancy losses occur at all temperatures above 1000^{o}C, and these losses increase with increasing quench temperature and decreasing quenching rate. This is in agreement with the results found in gold (Lengler 1976) and the results found in copper (Bourassa and Lengler 1976) where the vacancy losses were smaller and the Arrhenius plot more linear for the single crystal than for the polycrystal samples.

Since, as mentionned before, the purity of the polycrystals is the same as the single crystals, the difference in results

Figure 3.6 Comparison with Zetts and Bass'results.

Normalized resistance quenched into high purity platinum, using different quenching rates, as function of the inverse absolute quench temperature. Zetts and Bass'results have been chosen because the samples used have a purity, as measured by the residual resistivity ratio, comparable to the ones used in the present work.

◇ Water quench
△ Air quench
⊞ Kerosene quench
⊗ Helium gas quench
● Present work

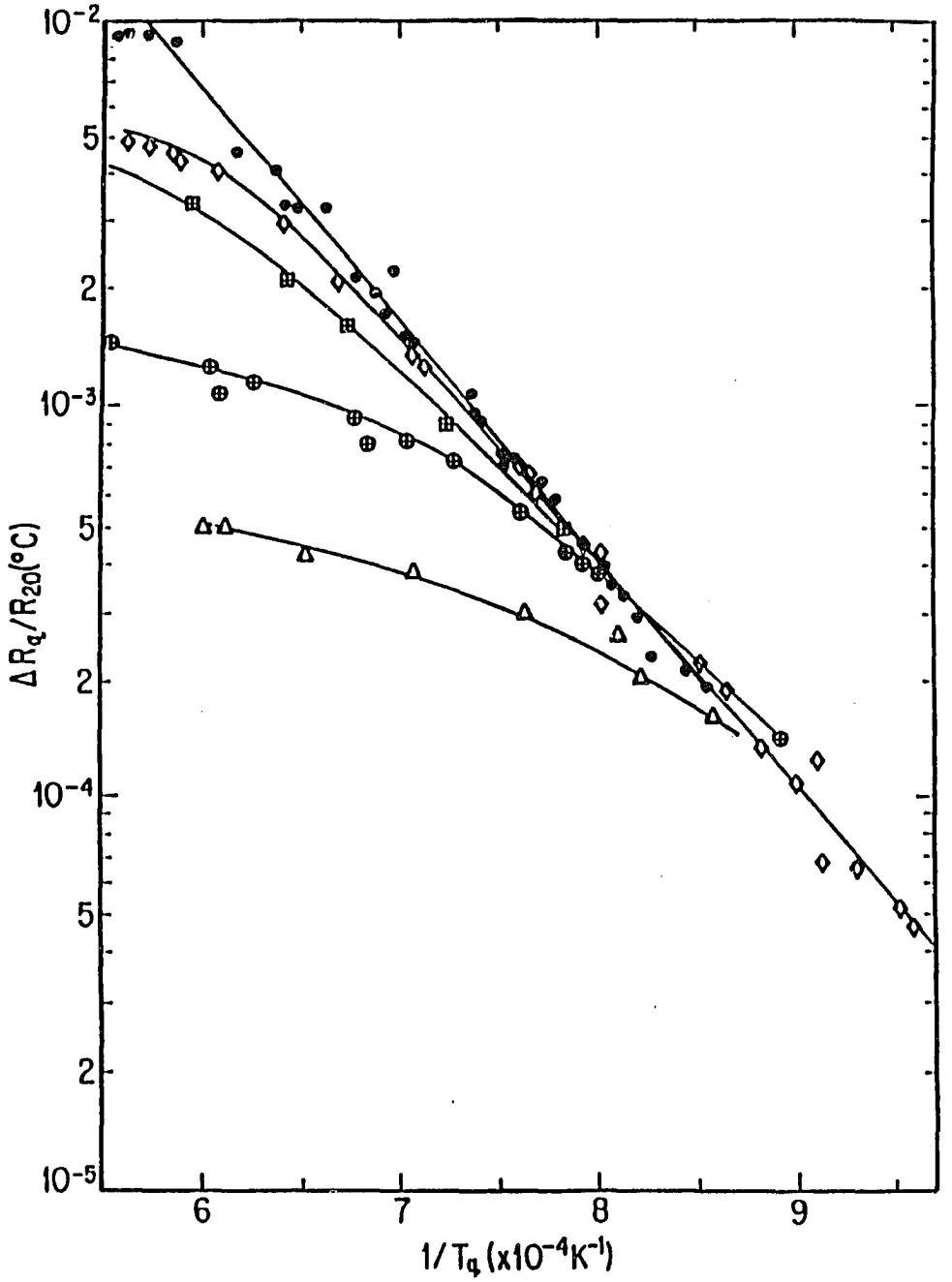

Figure 3.6 Comparison with Zetts and Bass'results.

should then be attributed to the dislocation density. In single crystals the dislocation density can be as low as 2000 cm/cm^3 (Lengler 1976),where for well annealed polycrystals it is in the range $5\times10^7 cm/cm^3$- $1\times10^8 cm/cm^3$ (Hull and Bacon 1984).

The fact that the single crystals with lower dislocation density trapped more vacancy concentration, as measured by the quenched-in resistance, is a confirmation that dislocations are the dominant sinks during quench as proposed by Seidman and Balluffi (1966), Balluffi, Lie, Seidman and Seigel (1969) and Emrick (1976).

Figure 3.7 represents the results of the model calculation of random parallel dislocation lines proposed by Emrick (1976). This figure shows the remaining fraction of the vacancy concentration as function of the dislocation density for quench rates from 160 °C/sec to 10^4 °C/sec. The quench temperature is 1500 °C. These results predict that rapid quenches are not necessary to trap the equilibrium vacancy concentration if the dislocation density is sufficiently low. A quench as low as 200 °C/sec from a quench temperature of 1500 °C traps essentially all the vacancies for dislocation densities as high as 10^4 cm/cm^3.

With the polycrystals quenched in air, the loss in quenched-in resistance is 48 % at 1000 °C, 82 % at 1200 °C, 89 % at 1300 °C and 93 % at 1400 °C. We have estimated these values assuming no loss in our extrapolated data. The air quenching rates used for these polycrystals vary between 400 °C/sec and 800 °C/sec (Zetts 1971). Using these values and the model calculation proposed by

Figure 3.7 Fraction of equilibrium vacancy concentration remaining as a function of dislocation density for quenching rates ranging from 100°C to 20,000 °C/sec. The quench temperature is 1500°C

The model is single vacancies migrating to a random array of parallel dislocation lines which maintain the instanteneous thermal equilibrium of vacancy concentration. E_m = 1.38 eV and $\nu = 1. \times 10^{13}$/sec.

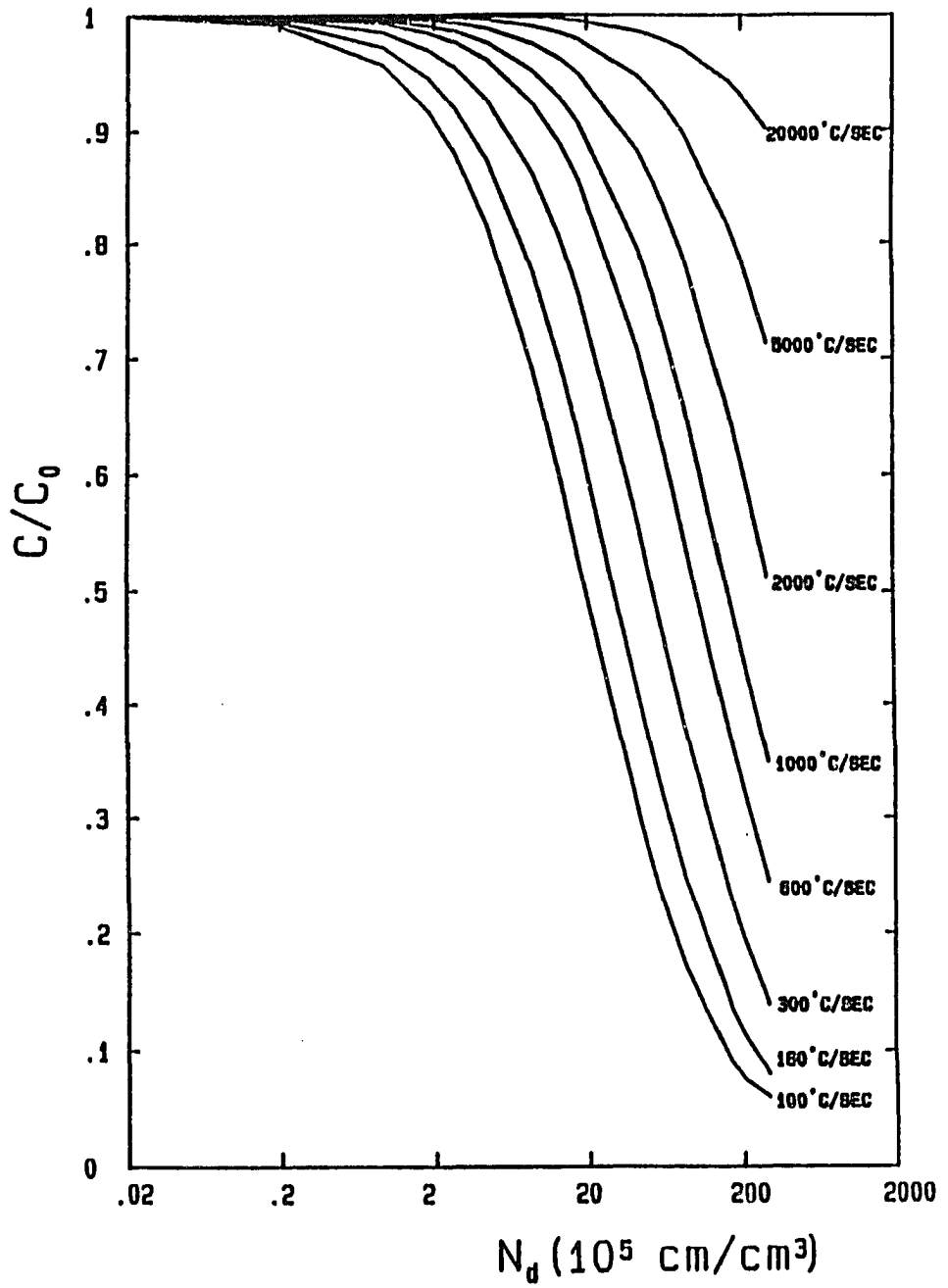

Figure 3.7 Fraction of equilibrium vacancy concentration remaining as a function of dislocation density for quenching rates ranging from 100°C to 20,000 °C/sec. The quench temperature is 1500°C

Emrick, we have found values in the interval(0.9-1.5) $\times 10^8$ cm/cm^3 for the dislocation density in the polycrystal samples. The actual dislocation density in these samples was not reported, however the value estimated is within the range of the dislocation density of a well annealed polycrystal sample. In contrast, the single crystal dislocation density has been estimated in section 1.2 to be no more than 10^6 cm/cm^3.

Using the same model, the linear water quenches, however, have yielded a slightly larger value, 2.5×10^8 cm/cm^3-4×10^8 cm/cm^3. This is to be expected since the water quenching rates being larger than the air ones would lead to the straining of the sample (Jackson 1965). The vacancy losses in the polycrystaline samples are 57 % at 1500°C, 40 % at 1400°C, 25 % at 1300 °C and 16 % at 1200 °C. The water quenching rates used vary from 5 10^4 °C/sec to 2×10^4 °C/sec.

The good agreement between the experimental results and the model calculation values is then strong evidence that dislocations are the main sinks for vacancies and that vacancy losses in nearly dislocation free samples are small.

2 PALLADIUM QUENCH

2.1. Results

Figure 3.8 displays the quenched-in resistance normalized to the resistance at 20 °C as function of the inverse of the absolute quench temperature. For quench temperatures below 1000

Figure 3.8 Normalized resistance quenched into single crystal of palladium as function of the inverse quench temperature.

LP represents the low purity samples results. PQ, the results determined using the optical pyrometer to measure the quench temperature.

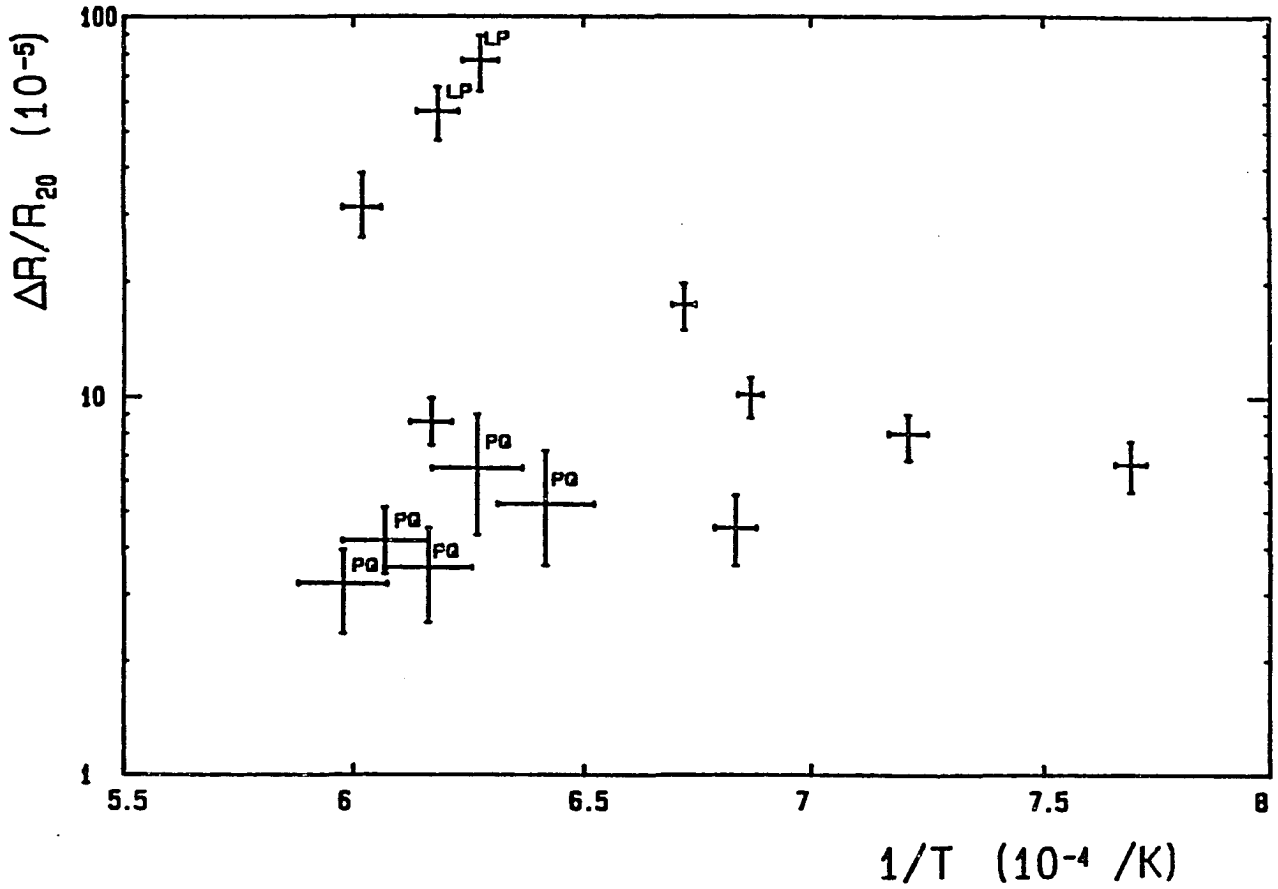

Figure 3.8 Normalized resistance quenched into single crystal of palladium as function of the inverse quench temperature.

^{o}C, the quenched-in resistance is too small to be measured with the present apparatus. To our knowledge there are no other data of quenched palladium to compare to the present data. Maier et al (1979) estimated the energy of formation of palladium by means of positron annihilation. They found it to be 1.85 $\pm$ 0.25 eV. Due the wide scattering of our data, no thermodynamic variable associated with point defects in quenched palladium could be derived. To improve the results, the samples were oriented along [110] and [100] but to no avail. However there are definitely vacancies quenched into the samples. For a quench temperature of of 1344^{o}C the quenched-in vacancy resistance was 0.23 $\mu\Omega$ for a sample with liquid helium resistance of 1.85 $\mu\Omega$. This represents a relative change in the resistance of 12 %, compared to a relative error in the measurements of the resistance in liquid helium of about 2 %. The change in the resistance due to quenching varies from 3 % to 18 % of the helium temperature value. By comparison, for platinum it is at least 25 %.

The quenched-in resistance is at least an order of magnitude smaller in palladium than in platinum or gold for similar relative temperatures. For a quench temperature of 0.71 Tm (Tm being the absolute melting temperature), the normalized quenched-in resistance, $\Delta R/R_{20}$, is 0.41×10^{-4} for palladium (present work), $1.78\ 10^{-3}$ for gold (Lengler 1976) and 1.99×10^{-3} for platinum (present work).

In a positron annihilation study of palladium Shaeffer (1982) found an equilibrium vacancy concentration at the melting

point of the order of 0.14×10^{-4}. Using the present quenched-in resistance values, we have found a palladium specific resistivity values in the range $(0.8\text{-}4.0) \times 10^{-4}$ μΩcm/at fract. These values are the same order of magnitude as the $1.6\ 10^{-4}$ μΩcm(at. fract.)$^{-1}$ value reported for gold (Lengler 1976) and the 4.6×10^{-4} μΩcm(at. fract.)$^{-1}$ value reported for platinum (Shaeffer 1982). The present low quenched-in resistance values found in palladium are then due to the large value, compared to that of gold and of paltinum, of its energy of formation.

We encountered in quenching palladium a green-blue oxide that forms on the sample after each anneal. This oxide affects the residual resitance ratio of the sample and it is sometime hard to get rid of.

In the first quenches, the temperature was measured by means of an optical pyrometer. The uncertainty in its measurement is of the order of 25 °C. As can be seen in Figure 3.8, the data obtained by this method are the poorest of all the palladium measurements.

Two quenches were made with low purity palladium (residual resistance ratio of the order of 170). These two quenches gave the largest values for the quenched-in resistance. This is to be expected since vacancy-impurity binding increases the equilibrium vacancy concentration as discussed earlier. The accuracy in the measurements of the quench temperature and of the resistances are of the same order of magnitude as those of platinum in the rf furnace. The accuracy of these measurements has already been

discussed in section 1.5.1. Since the change between the quenched and the annealed sample resistances is much smaller, the uncertainty on the quenched-in resistance is at least twice as large. The uncertainty in the resistance increment is more than 30 %.

2.2. Future Work

Because of its high sensitivity to defects, the dHvA phenomenon could be used to study the effect of vacancies on the scattering of the conduction electrons. The scattering of the electrons by vacancies manifests itsef as an apparent temperature known as the Dingle temperature. Previous studies (Lengler 1976, Shoenberg 1984) have shown that the major effect of defects on probing of the fermi surface is to cause a "phase smearing" of the signal. This results in an exponential damping of the de Has-van Alphen signal amplitude and an increase in the Dingle temperature.

Single crystals of high purity and low dislocation densities are needed for this study. The present quenching technique provides such high quality samples. Only vacancies and divacancies distributed randomly are qenched-in by this new procedure. The present technique is an improvement over Lengler's. Lengler's rapid cooling of the samples leads to lattice strain, thus to an increase in the dislocation density (Lengler 1977). In our case, the samples are cooled at slow rate avoiding strain.

3. PALLADIUM RESISTANCE AS FUNCTION OF TEMPERATURE

3.1. Solid Palladium Resistance

Figure 3.9 shows the palladium single crystal resistance as a function of temperature. The squares represent the experimental data and the solid line a linear regression fit of these data. The results have been normalized by the room temperature resistance so as to correct for size variation between samples. The fitting done to the relation

$$R(T) = R_{22}(A_0 + A1T + A_2T^2 + A_3T^3) \text{ gives}$$

$$A_0 = 0.9301 \pm 0.0042$$

$$A_1 = (0.3627 \pm 0.0006)\ 10^{-2}/^{\circ}C$$

$$A_2 = (-0.1235 \pm 0.0010)\ 10^{-5}/^{\circ}C^2$$

$$A_3 = (0.2039 \pm 0.0047)\ 10^{-9}/^{\circ}C^3$$

$R(T)$ and R_{22} being the resistance at temperature T and at temperature 22 $^{\circ}$C respectively. The reduced χ^2 and the value of F for test of fit for the above were 0.5 and 3.7×10^5 respectively. For a 3 parameter fit they were 2.5 and 1.0×10^5 respectively .

The graph of the resistance versus temperature bends away from linearity toward the temperature axis. The bending can be explained by the effect of sharp structure in the electronic density of states on the interband s-p phonon scattering (Fradin 1974). Below 650 $^{\circ}$C, deviation from the results of Laubitz and Matsamura (1972) are too small to be shown on the graph. Above 650 $^{\circ}$C to their upper limit of 1030 $^{\circ}$C, our values are 0.5 %

Figure 3.9 High purity single crystal palladium resistance as function of temperature.

The dots represent the data points. The line, a least-squares fit of these data.

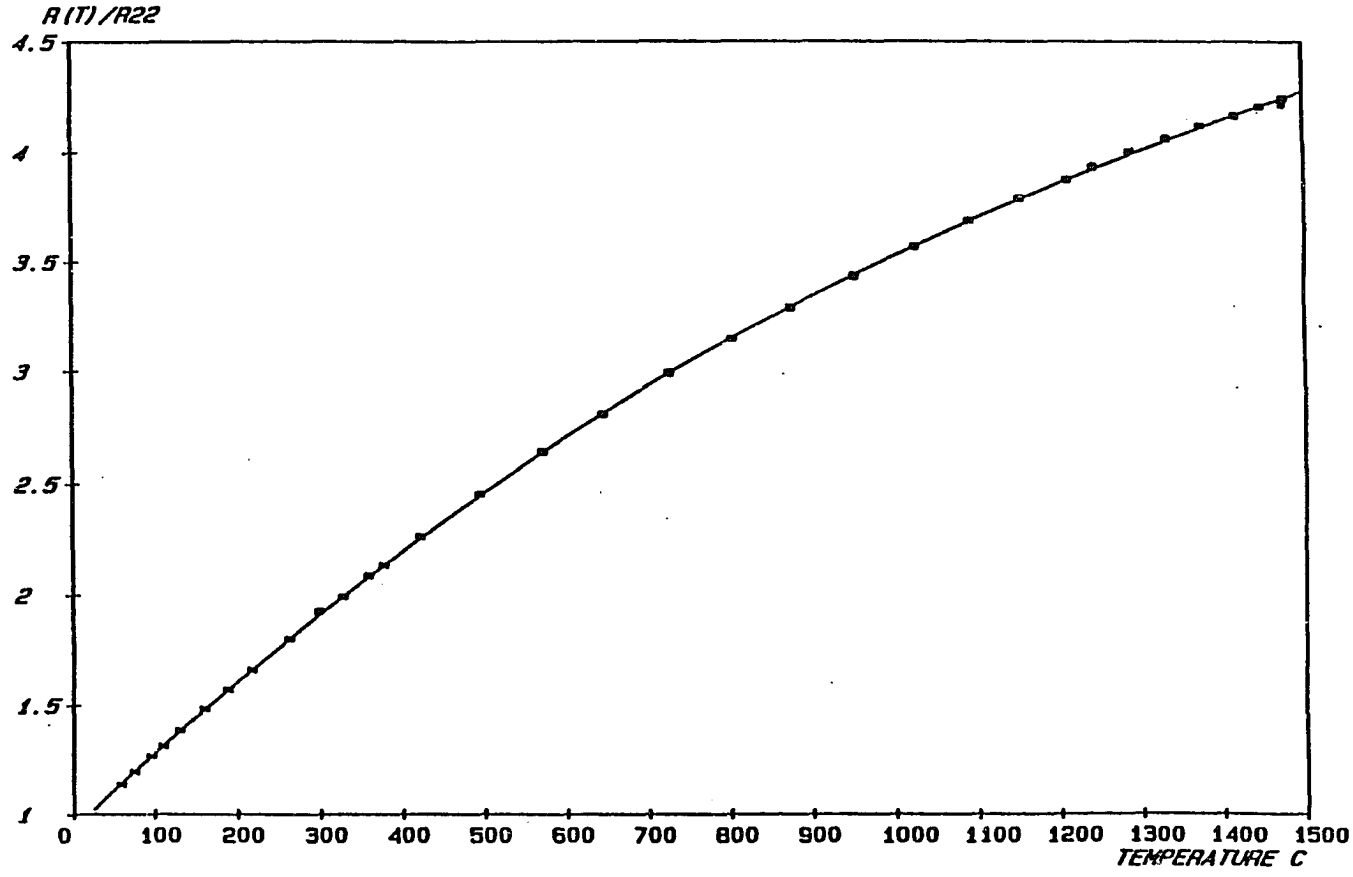

Figure 3.9 High purity single crystal palladium resistance as function of temperature.

lower. More extended results were reported by Guntherodt et al. (1975) and Dupree et al. (1975).

Due to the large uncertainty in the measurement of the diameter of their samples, Dupree et al. (1975) normalized their data to those of Laubitz and Matsumura (1972). Up to 1030 °C their results are then identical to Laubitz and Matsumura. Above 1030 °C the graph can not be read accurately enough to make a comparison. However if we use their ratio of the liquid to solid resistivity and their value of the molten sample resistivity, we found that our solid sample resistivity at the melting point is 2.5 % to 5 % lower.

In the work of Guntherodt et al. (1975), essential details are missing. The sample treatement and purity were not reported. The experimental procedures were not described. Their results were present in a graph, but this graph can not be read accurately enough to make a meaningful comparison.

The room temperature resistance R_{22} and the high temperature resistance R(T) were measured with a precision better than 0.1 %. The experimental accuracy is limited by the uncertainties in the determination of the temperature. The main contribution to the error comes from the temperature gradient along the gauge region. This gradient, varying between 2 °C and 5 °C, was not constant but a function of the measuring temperature. These variations are shown in Figure 3.10. We estimated the error in the temperature measurements to be of the order of 1 %.

Table 3.4 Molten palladium resistivity.

ρ ($\mu\Omega$cm)	Method	Reference
41.6	Theoretical hard sphere model	Brown (1973)
62	Calculated using the liquid structure factor of Ni	Brown (1973)
70-80	Estimated value based on Vines (1941) 100°C experimental data	Brown (1973)
83 ± 2	Experimental	Dupree et al. (1975)
79	Experimental	Guntherodt et al. (1975)
77.3 ± 1.0	Experimental	Present work

3.2. Liquid Palladium Resistance

The molten palladium resistance normalized to room temperature resistance was found to be :

$$R_m/R_{22} = 7.33 \pm 0.09$$

The resistivity of the molten palladium was estimated from the above normalized resistance and the room temperature resistivity. The room temperature resistivity was found to be $\rho_{22} = 10.55 \pm 0.11\,\mu\Omega cm$, and was measured using a palladium single crystal with a residual resistivity ratio better than 25,000. The major contribution to the uncertainty comes from the measurement of the length of the sample. The diameter was measured with a traveling microscope to within $2.5\ 10^{-3}$ mm.

In Table 3.4 our value of the molten palladium resistivity is reported along with early experimental results by Dupree et al. (1975) and Guntherodt et al. (1975), and theoretical predictions by Brown (1973). Our results are in good agreement with those of Guntherodt et al. (1975). They are about 5 % lower than those of Dupree et al. (1975). However, since our ratio of the liquid to solid resistivity is nearly the same as theirs, the difference may then be due to the normalization to the solid resistivity. All of the experimental liquid metal resistivities are reasonably close to the calculated values, based upon the muffin-tin phase shift treatment, reported by Brown (1973).

In going through the melting point, the resistance increased

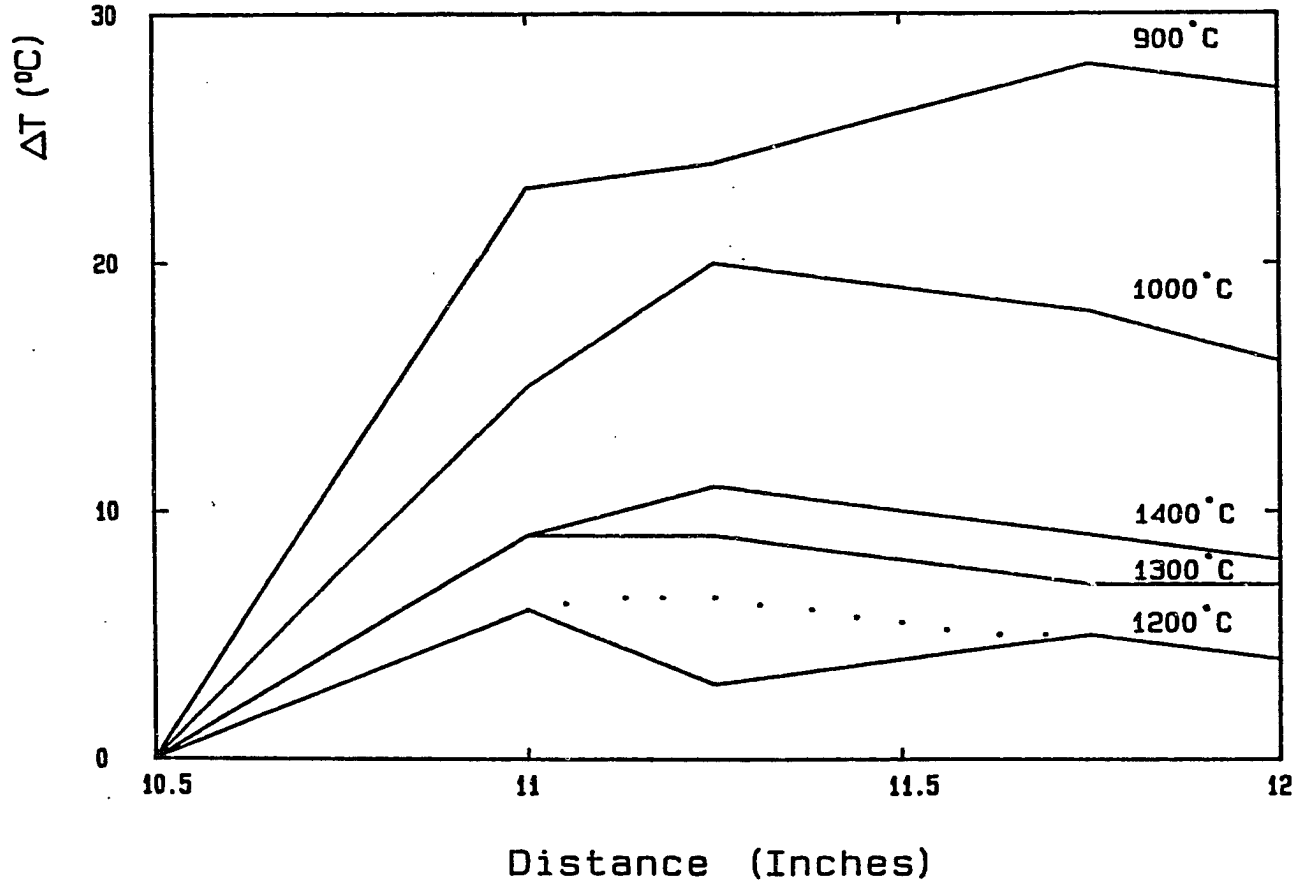

Figure 3.10 HR furnace vertical temperature gradient as function of the measuring temperature.

by a factor of 1.71. This value is in good agreement with that of Dupree et al. (1975). In Table 3.5, we have reported the increase in resistivity upon melting of the transition metals studied to date. This table shows that this increase is larger in palladium than any other transition metal. This fact has been explained (Wilson 1965, ten Bosch and Bennemann 1975) by the considerable drop in the d band contribution to the conductivity in going through the transition metal series to palladium. Presumed less sensitive to melting than that of the s band, the d band contribution to conductivity should reach a maximum when the d band is half filled.

Table 3.5_ Change in the resistivity of transition metals going through the melting point.

Metal	$\frac{\rho_l}{\rho_s}$	$\frac{\rho_l - \rho_s}{\rho_s}$	Reference
Fe	1.09	9 %	Powell (1953)
	1.06	6 %	Guntherodt et al (1975)
Co	1.20	20 %	Guntherodt et al (1975)
Ni	1.30	30 %	Lebedev (1968)
	1.47	47 %	Guntherodt et al (1975)
Mo	1.23	23 %	Lebedev (1968)
Rh	1.57	57 %	Martynyuk and Tsapkov (1974)
Pd	1.70	70 %	Dupree et al (1975)
	1.71	71 %	Present work
W	1.08	8 %	Lebedev (1968)
Ir	1.30	30 %	Martynyuk and Tsapkov (1974)
Pt	1.40	40 %	Lebedev (1968)
	1.49	49 %	Martynyuk and Tsapkov (1974)
	1.42	42 %	Van Zytveld (1980)

CHAPTER IV

CONCLUSIONS

We have developed a technique to produce and quench large diameter, high purity, low dislocation density samples. This technique is an improvement over previous ones in that, unlike the others, it eliminates the introduction of unwanted dislocations during quench. A new crystal is grown each time and is not handled until after the slow air quench.

We have applied this technique to quench high purity platinum single crystals. The results show that we have been able to drastically reduce the vacancy losses that usually occur at temperatures above 1000 °C. We have found the energy of formation of vacancies to be $E_f = (1.30 \pm 0.03)$ eV. The entropy of formation and the concentration of vacancies at the melting point have been estimated to be respectively $S_f = (0.42 \pm 0.11)k$ and $C_v(T_m) = (9.4 \pm 0.7)\times10^{-4}$.

We have analysed our data using a model sink for vacancies loss proposed by Emrick. It is a cylindrical model where the core has been assumed to drain the cylindrical volume. We have found that our results are in agreement with the model predictions. We have also found that the model results are consistent with previous quenching data for platinum.

We have also quenched high purity palladium single crystals

by the same method. Although, an increase in resistance has been observed, it has been impossible to determine any thermodynamic variable associated with vacancies in palladium because of the scattering of the data. In an effort to improve our results, we have oriented our crystal samples but to no avail.

We believe that the quenched samples are ideal for the study of the scattering of electrons by vacancies using the dHvA technique. "Dingle temperature" is a measure of this scattering. The vacancy concentration can be inferred from Dingle temperature. Since the samples are high purity and nearly dislocation free, the effect of point defects can be studied separately.

Due to the need for a temperature scale, we have also measured with high accuracy the resistance of an ultra pure palladium single crystal to within 100°C of the melting point. The variation of the resistance with temperature is of the form:

$$R(T) = R_{22}(A_0 + A_1T + A_2T^2 + A_3T^3)$$

with

$A_0 = 0.9301 \pm 0.0042$

$A_1 = (0.3627 \pm 0.0006)\ 10^{-2}/^{\circ}C$

$A_2 = (-0.1235 \pm 0.00010)\ 10^{-5}/^{\circ}C^2$

$A_3 = (0.2039 \pm 0.0047)\ 10^{-9}/^{\circ}C^3$

We have also measured the molten palladium resistivity. We have found it to be (77.30 ± 1.0) $\mu\Omega$cm. The increment in the resistivity by melting have been determined to be 1.71.

In conclusion, the present quenching method permits the preparation of samples where the effect of vacancies in general

can be studied separately from that of other kinds of defects.

APPENDIX A

RESIDUAL RESISTIVITY RATIO

Because of its sensitivity to impurities and the simplicity of its measurement, the electrical resistivity at low temperature is a convenient parameter to use to estimate the purity content of materials. The method is based on Matthiessen's rule. As discussed in chapter I, according to this rule, the resistivity of a metal is approximately the sum of the intrinsic resistivity due to the scattering of electrons by thermal vibrations of the lattice and by the electrons, and the residual resistivity due to scattering by impurities and lattice defects.

At liquid helium temperature, we have the following effects

1. The intrinsic resistivity becomes very small compared to the room temperature value. At this temperature, it is mainly due to electron-electron scattering. In transition metals, the contribution of the electrons to the resistivity arises from the scattering of the low-mass, mobile s-band electrons by the relatively heavy, nearly stationary d-band (Mott 1964). This effect is rather important in palladium because the density of electronic states at the Fermi level is very high. Neglecting the phonon contribution, the resistivity at helium temperature is

$$\rho(T) = \rho_0 + AT^2 \qquad (1)$$

where ρ_0 is the resistivity due to impurities and lattice defects, T the absolute temperature. AT^2 is the resistivity due to the electron-electron scattering. In palladium AT^2 represents as much as 50 % of the total resistivity at helium temperature.

2. The residual resistivity becomes preponderant. In a well-annealed sample, the contribution of the point defects to this resistivity is negligible. The contribution of dislocations of a typical density of 10^7 cm/cm^3 is also insignificant. The surface plays however an important role, especially in high purity and thin samples. The mean free path of conduction electrons, L, increases as the temperature is lowered and the scattering centers, created by impurities and defects, are reduced. This increase in the mean free path enhances the influence of the sample surface on the bulk conductivity. As the diameter, d, of the sample approaches the mean free path, a significant fraction of conduction electrons will be scattered at the surface. In the case where d>>L, the residual resistivity is given by (Blatt 1968)

$$\rho_0 = \rho_b \left[1 + \frac{3}{4} \frac{L_{4.2}}{d} \right] \qquad (2)$$

where $L_{4.2}$ is the mean free path at liquid helium temperature, d the diameter of the sample and ρ_b is the bulk resistivity. In a well-annealed, nearly dislocation free sample ρ_b is the resistivity due to impurities.

In such a sample, two corrections should then be made to the resistivity at liquid helium temperature to get a proper estimate

of the resistivity due to impurities:

1. a temperature correction due to electron-electron scattering
2. a size correction due to surface scattering

Using equations (1) and (2), the residual resistivity due to imputies will then be:

$$\rho_b = \frac{\rho_T - AT^2}{1 + \frac{3}{4}\frac{L_{4.2}}{d}}$$

In pratice, to eliminate the sample shape factor, the purity of the sample is estimated using the residual resistivity ratio, i.e., the ratio of the resistivity at room temperature, ρ_{300}, to resistivity due to impurities, ρ_b. In this case we have using equation (3):

$$\frac{\rho_{300}}{\rho_b} = \frac{\rho_{300}}{\rho_T - AT^2}\left[1 + \frac{3}{4}\frac{L_{4.2}}{d}\right]$$

assuming $\frac{R_{4.2}}{R_{300}} = \frac{\rho_T}{\rho_{300}}$

$$RRR = \frac{\rho_{300}}{\rho_b} = \frac{1 + \frac{3}{4}\frac{L_{4.2}}{d}}{\frac{R_{4.2}}{R_{300}} - \frac{AT^2}{\rho_{300}}} \qquad (4)$$

R_{300} being the room temperature resistance and $R_{4.2}$ the liquid helium resistance.

In the present work, we used equation (4) to determine the residual resistivity ratios of our samples. R_{300} and $R_{4.2}$ were measured, d was 1mm and the other parameters used are presented in Table A.1. The mean free path at liquid helium temperature is determined from that at nitrogen temperature by assuming that it is inversly proportional to the resistivity.

Table A.1: Residual resistance ratio correction parameters

Parameter	Platinum	palladium	Reference
Temperature coefficient,A (10^{-11} μΩcm/K)	1.4	1.59	White and Woods (1959) Webb et al (1979)
Mean free path,L, at 77k, (in A)	500	1250	Panchenko et al (1969)
Resistivity at 77 K (μΩcm)	1.79	1.59	Panchenko et al (1969)
Resistivity* at 300 K (μΩcm)	10.88	10.73	Flynn and O'Hagan(1967) Present work

* the values reported have been converted from the 293 K value for platinum and the 295 K value for palladium

In the present work the residual resistivity ratio is assumed to be proportional to the total impurity content (Caron 1955). Our results are reported in chapter II. However these results are just an approximation since the relative proportions of the impurities present in the zone-refined samples are not known. Another rough estimate of the impurity content of a sample from the residual resistivity ratio is to take the total impurity content in the range of 1 ppm when the residual resistivity ratio is 10,000 (Misek 1970, Bass 1972).

APPENDIX B

SINK MODEL FOR VACANCY LOSS

Vacancy loss during quenching has been studied both theoretically and experimentally (Flynn et al 1965, Seidman and Balluffi 1965, Perry 1970, Polak 1974, Emrick 1976, 1978). As mentioned in chapter I, sink models have been regular and random arrays of point sinks, dislocation lines and cell-surfaces (approximated by spheres). An analysis of all these models has been reported by Emrick (1978). Their applicability has been discussed in chapter I.

The standard method for finding the retained vacancy concentration is to solve the diffusion equation (Carslaw and Jaeger 1949)

$$\frac{\partial C}{\partial t} = D_v(t)\, \nabla^2 C \qquad (1)$$

subject to the boundary conditions dictated by the model. In the above equation C_v is the concentration of vacancies and $D_v(t)$ is the vacancy diffusion coefficient given by

$$D_v(t) = D_{ov}\exp(-E_m/kT(t)) \qquad (2)$$

with E^m the migration energy and T(t) is the temperature of the

sample at time t.

The model used in this study has been developed by Emrick (1976,1978). It is a random array of dislocation lines of core radius a draining a cylinder of radius b. This model should reasonably bracket the dislocation structure in well-annealed samples. However the spherical model, where the surface is the sink draining the included volume, is more accurate for samples with larger dislocation densities (Emrick 1978). In the dislocation lines model, it has been assumed that the sink maintains the instantaneous thermal equilibrium vacancy concentration as the sample cools from the quench temperature Tq at a constant rate τ_q to a temperature at which the vacancies are essentially immobile. The boundary conditions, including the time-dependent equilibrium boundary conditions are:

$$\begin{aligned} C_v &= \exp(S_f/k)\,\exp(-E_f/kT(t)) && t>0 && r = b \\ \frac{\partial C_v}{\partial r} &= 0 && \text{all } t && r = a \\ C_v(Tq) &= C_v{}^0 && t = 0 && a < r < b \end{aligned} \qquad (3)$$

where E_f and S_f are the energy and entropy of formation respectively.

A solution to equation (1) subject to the boundary conditions of equation (3) yields

$$C_v\,(r,T(t)) = \sum_{n=0}^{\infty} \beta_n\, U_0(\alpha_n r) \qquad (4)$$

where $U_0(\alpha_n r) = Y_0(\alpha_n a)\, J_0(\alpha_n r) - Y_0(\alpha_n r)\, J_0(\alpha_n a)$

and

$$\beta_n = \frac{2aC_0}{\alpha_n} \frac{J_0(\alpha_n a)\, Y_1(\alpha_n a) - J_1(\alpha_n a)\, Y_0(\alpha_n a)}{b^2[J_0(\alpha_n b)\, Y_0(\alpha_n a) - J_0(\alpha_n a)\, Y_0(\alpha_n b)]^2 - a^2[J_1(\alpha_n a)\, Y_0(\alpha_n a) - J_0(\alpha_n a)\, Y_1(\alpha_n a)]^2}$$

with $J_n(x)$ and $Y_n(x)$ being Bessel Functions of the first and second kind of order n. The α_n are the zeros of

$$J_1(\alpha_n b) Y_0(\alpha_n a) - J_0(\alpha_n a) Y_1(\alpha_n b) = 0$$

As its distribution is random, the probability density for the cylinder radii is given by

$$P(b) = 2\pi bK \exp(-\pi b^2 K) \qquad (5)$$

where K is the mean dislocation density. The initial number of vacancies in a cell of radius b is then

$$N = C(T_q, \tau_q, b)\pi b^2 L$$

Using the above relation and equations (4) and (5), the average fraction of vacancies remaining is

$$C(T_q, \tau_q) = \frac{\int_0^\infty NP(b)d(\pi b^2 L)}{\int_0^\infty P(b)d(\pi b^2 L)}$$

$$C(T_q,\tau_q) = \frac{\int_0^\infty \exp(-\pi b^2 k) C(T_q,\tau_q,b) b^3 db}{\int_0^\infty \exp(-\pi b^2 k) b^3 db} \qquad (6)$$

To obtain the vacancy concentration as function of the dislocation density for different quenching rates and different quench temperature, equations (4) and (6) have been evaluated on a computer.

For water quench, the quenching rates have been linear, i.e., $T(t) = T_q(1 - t/\tau_q)$; while for air quench, they have been exponential, i.e, $T(t) = T_q \exp(-t/\tau_q)$. Since divacancies represent only 6 % of the total concentration their effect has not been taken into account. The ambient temperature has been taken to be 100°C. The loss calculations have been insensitive to the choice of values between 0°C and 250°C.

For the energy of migration, we have used the 1.38 eV value determined from a self-consistent fit of quenching and diffusion data by Schumacher et al (1978). The frequency factor has been taken to be 1.0×10^{13} /sec. These values have been used because they have given dislocation densities in a well-annealed platinum comparable with those observed in well-annealed gold (Emrick 1982).

REFERENCES

Ascoli, A.,M. Ascente, E. Germagnoli, and A.Manara (1958) J.Phys.Chem.6, 59.

Bacchella, G.L., E. Germagnoli and S. Granata (1954) J.Appl. Phys.30, 748.

Balluffi, R.W., K.H. Lie, D.N. Seidman and R.W. Siegel (1970) Vacancies and Interstitials in Metals p125 (Seeger, A., D.Schumacher, W. Schilling and J. Diehl, eds) North Holland Publ. Co.

Bass, J.,(1972) Adv. Phys. 21,431

Berger, A.S., D.N. Seidman and R.W. Balluffi (1973) Acta Met.21, 137.

Blatt, F.J.,(1968) Physics of Electronic Conduction in Solids, p 199, Mc Graw Hill, New York.

ten Bosch,A. and K.H. Bennemann (1975) J.Phys. F5, 1333.

Bradshaw, F.J. and S. Pearson (1956) Phil.Mag.1, 812.

Brandt, W. (1967) Positron Annihilation, p 178 (Steward, A.T. and L.O. Roelling, eds) New York.

Brown, J.S.(1973) J.Phys. F3, 1003.

Burke, J. (1972) J. Less-Common Metals 28, 441.

Caron, M. (1955) Publ. Sci. Tech. Min. Air 328 Paris.

Carslaw, H.C. and J.C. Jaeger (1947) Conduction of Heat in

Solids, Oxford University Press.

Charles, M., J. Hillairet, M. Beyeler and J Delaplace (1975) Phys. Rev.B11, 4808.

Chang, Y.K. and R.J. Higgins (1975) Phys. Rev. B12, 4261.

Cotterill, R.M.J. and R.L. Segall (1963) Phil. Mag. 8 , 1105.

Dekhtyar, I.Ya. and V.S. Mikhalenkov (1964) Soviet Phys.-Solid State 5, 2193.

Dupree, B.C., J.B. Van Zytveld and J.E. Enderby (1975) J.Phys.F 5 L200.

Dlubek, G., O. Brummer and N Meyendorf (1977) Appl. Phys. 13, 67.

Emrick, R.M. (1976) Phil.Mag. 33, 277.

Emrick, R.M. (1978) Phil. Mag. 37, 355.

Emrick, R.M. (1978) J. Phys. F8, 1353.

Emrick, R. M. and J J Vuillemin (1981) Bull.Am.Phys.Soc. 26, 473.

Emrick, R.M. (1982) J. Phys. F12, 1327.

Esposito, E., H. Ehrenreich and C.D.Jr Gelatt (1978) Phys. Rev. B18, 3913.

Evans, R., D.A. Greenwood and P. Lloyd (1971) Phys. Lett. 35A,57.

Eyre, B.L., M.N. Loretto and R.E. Smallman (1977) Vacancies'76, (Smallman, R.E. and J.E. Harris,eds) The Metal Society.

Flynn, C.P. (1962) Phys. Rev. 126, 533.

Flynn, C.P. (1964) Phys. Rev. 134A, 341.

Flynn, C.P., J. Bass and D. Lazarus (1965) Phil. Mag. 11, 521.

Flynn, C.P. (1972) Point Defects and Diffusion, Clarence Press, Oxford.

Flynn, D.R. and M.E. O'Hagan (1967) J. Res. NBS C71, 255.

Gersriken, S.D. and N.N.Novikov (1960) Fiz. Metal. Metalloved. 9, 224.

Guntherodt, H. J., E. Hanser, H.U. Kunzi and R. Muller (1975) Phys.Lett. 54A, 291.

Ham, F.S. (1959) J. Appl. Phys. 30,915.

Heigel, F. and R. Sizman (1972) Cryst. Latt. Defects 43A, 289.

Hull, D. and D. J. Bacon (1984) Introduction to Dislocations, 3rd ed. Pergamon Press,New York

Jackson, J.J. (1963) Acta Met. 11,1245.

Jackson, J.J. (1965) Lattice Defects in Quenched Metals p467 (Cotterill, R.M., M. Doyama, J.J. Jackson and M Meshii, eds) Academic Press, New York.

Kopan, V.S. (1965) Fiz. Met. Metalloved. 19, 569.

Kraftmakher, Ya.A. and E.B. Lanina (1965) Soviet Phys. Solid state 7, 92.

Laubitz, M.J. and T. Matsumura (1972) Can. J. Phys. 50, 196.

Lazarev, B.G. and O.N. Ovcharenko (1954) Soviet Phys. JETP 36(9), 42.

Lebedev, S.V. (1968) High Temp. 6, 150.

Lengler, B. (1976) Phil. Mag. 34, 259.

Lengler, B. (1977) Phys. Rev. B15, 5504 .

McKenzie, I.K., T.L. Khoo, A.B. MacDonald and B.T.L. McKee (1967) Phys. Rev. Lett. 19, 946.

Maier, K., G. Rein, B. Saile, P.Valenta and H.E. Schaeffer (1979)

Proc. 5th Int. Conf. on Positron Annihilation (Japan).

Martynyuk, M.M. and V.I. Tsapkov (1974) Fiz. Metal. Metalloved. 37, 49.

Misek, K. (1970) Czech. J. Phys. B20, 1214.

Misek, K. (1979) Czech. J. Phys. B29, 1243.

Mott, N.F. (1964) Adv. Phys. 13, 325.

Mott, N.F. (1972) Phil. Mag. 26, 1249.

Muller, E.W. (1959) Z. Physik. 156, 399.

Panchenko, O.A., P.P. Lutsisshin and Yu.G. Ptushinskii (1969) Soviet Physics JETP 29, 76.

Perry, A.J. (1970) Phil. Mag. 21, 743.

Petroff, P. and D.N. Seidman (1971) Cornell University Materials Science Center Report.

Polak, J. (1974) Cryst. Latt. Defects 5, 155.

Powell, R.W. (1953) Phil. Mag. 44, 772.

Rattke, R., O. Hauser and J. Wieting (1968) Phys. Stat. Sol. 31, 167.

Sandesara, N.B. and J.J. Vuillemin (1977) Metall. Trans. 8B, 693.

Schaeffer, H.E. (1982) Positron Annihilation p369 (Coleman, P.G. S.C. Sharma and L.M. Diana, eds) North Holland Publ. Co.

Schumacher, D., A. Seeger and O. Harlin (1968) Phys. stat. sol. 25, 359.

Seeger, A. (1962) J. Phys. Radium 23, 616.

Seeger, A. and H. Mehrer (1968) Phys. Stat. Sol. 29, 231.

Seeger, A. and H. Mehrer (1970) Vacancies and Interstitials in Metals, p 1 (Seeger, A., D. Schumacher, W. Schilling and J. Diehl, eds) North Holland Publ. Co. Amsterdam.

Seidman, D.N. and R.W. Balluffi (1965) Phys. Rev. 139A, 1824.

Seidman, D.N. and R.W. Balluffi (1966) Phys. Stat. Sol. 17, 531.

Seidman, D.N. and R.W. Balluffi (1967) Lattice Defects and their Interactions, p 911 (Hasiguti, R.R., ed) Gordon and Breach, New York.

Siegel, R.W. (1978) J. Nucl. Mat. 69 & 70, 117.

Simmons, R.O. and R.W. Balluffi (1960) Phys. Rev. 119, 600.

Simmons, R.O. and R.W. Balluffi (1962) Phys. Rev. 125, 862.

Simmons, R.O. and R.W. Balluffi (1963) Phys. Rev. 129, 1533.

Shoenberg, D. (1984) Magnetic Oscillations in Metals Cambridge University Press, New York.

Takamura, J. (1961) Acta Met. 9, 547.

Takamura, J. (1963) J. Phys. Soc. Japan 18, Suppl. III,7.

Van Zytveld, J.B. (1980) J. Phys. 41, Suppl.8,C8-503.

Webb, R.A., G.W. Crabtree and J.J. Vuillemin (1979) Phys. Rev. Lett. 43, 796.

White, G.K. and S.B. Woods (1959) Trans. Roy. Soc. London 251A, 273.

Wilson, J.R. (1965) Metall. Rev. 10, 381.

Zetts, J.S. (1972) Thesis Univ. of Michigan.

Zetts, J.S. and J. Bass (1975) Phil. Mag. 31, 419 .